

In-situ Atomic Layer Deposition growth of Hf-oxide

Von der Fakultät für Mathematik, Naturwissenschaften und Informatik
der Brandenburgischen Technischen Universität Cottbus

zur Erlangung des akademischen Grades

Doktor der Naturwissenschaften
(Dr. rer. nat.)

genehmigte Dissertation

vorgelegt von

Diplom-Physiker

Konstantin Karavaev

geboren am 03.02.1982 in Kemerovo, Russland

Gutachter: Prof. Dr. rer. nat. habil. Dieter Schmeißer

Gutachter: Prof. Dr. rer. nat. habil. Ehrenfried Zschech

Gutachter: Prof. Dr. rer. nat. habil. Christian Pettenkofer

Tag der mündlichen Prüfung: 17 Juni 2010

To my parents and my girlfriend Annabel

Acknowledgements

This thesis is based on the experimental work carried out in the Chair Applied Physics and Sensors, Brandenburg University of Technology Cottbus and BESSY, during the years 2006-2009.

I wish to express my deep gratitude to my supervisor Professor Dieter Schmeisser for his support, encouragement and advice during this work. I would like to thank my coauthors Dr. Massimo Tallarida for sharing his experience and immeasurable help throughout the course of this work. For technical help and assistance, I wish to acknowledge Mr. Guido Beuckert and Mrs. Ioanna Paloumpa. The whole personnel in the Chair Applied Physics and Sensors, Brandenburg University of Technology Cottbus.

The International Graduate School at BTU Foundation are acknowledged for the financial support. My warmest thanks belong to my family, especially my mother Tamara Karavaeva, my father Sergey Karavaev and my girlfriend Anna Monakhova and my friends for their support.

Cottbus, December 2009

Karavaev Konstantin

Abstract

We have grown HfO_2 on $\text{Si}(001)$ by atomic layer deposition (ALD) using HfCl_4 , TEMAHf , TDMAHf and H_2O as precursors. The early stages of the ALD were investigated with high-resolution photoelectron spectroscopy and x-ray absorption spectroscopy. We observed the changes occurring in the $\text{Si}2p$, $\text{O}1s$, $\text{Hf}4f$, $\text{Hf}4d$, and $\text{Cl}2p$ (for HfCl_4 experiment) core level lines after each ALD cycle up to the complete formation of two layers of HfO_2 . The investigation was carried out in situ giving the possibility to determine the properties of the grown film after every ALD cycle or even after a half cycle.

This work focused on the advantages in-situ approach in comparison with ex-situ experiments. The study provides to follow the evolution of the important properties of HfO_2 : contamination level, density and stoichiometry, and influence of the experimental parameters to the interface layer formation during ALD.

Our investigation shows that in-situ XPS approach for ALD gives much more information than ex-situ experiments.

Contents

Abstract	v
Contents	vii
1 Introduction	1
1.1 MOSFET performance and scaling	1
1.2 High-k gate dielectric	3
1.3 In-situ approach of investigation high-k oxide	7
2 Basics	9
2.1 Atomic Layer Deposition	9
2.2 X-ray Photoelectron Spectroscopy	11
3 Experimental	15
3.1 The ALD in-situ system	15
3.2 In-situ XPS and XAS system at BESSY	17
3.3 Used Precursors	19
4 Results and discussion	21
4.1 Ex-situ investigation of industrial layers of Hf-oxide on Si by X-ray Photoelectron Spectroscopy	21
4.2 Investigation of in-situ layers by XPS, XAS	23
4.2.1 Quantitative analysis	23
4.2.2 Evolution of interfaces HfO ₂ /SiO ₂ /Si	27
4.2.3 Model of growth	28
4.2.4 Physical properties in-situ prepared layers of Hf-oxide	30
4.2.5 Contamination content in the HfCl ₄ experiment	35
4.3 In-situ study of individual steps of ALD process	38
5 Conclusions	41

Bibliography	45
List of publications	49
List of Symbols and Abbreviations	51
List of Figures	53
List of Tables	57

Chapter 1

Introduction

1.1 MOSFET performance and scaling

The industry's demand for greater integrated circuit functionality and performance at lower cost requires an increased circuit density, which has translated into a higher density of transistors on a wafer [1]. This rapid shrinking of the transistor feature size has forced the channel length and gate dielectric thickness to also decrease rapidly. The improved performance associated with the scaling of logic device dimensions can be seen by considering a simple model for the drive current associated with a FET [2]. The drive current can be written (using the gradual channel approximation) as

$$I_D = \frac{W}{L} \mu C_{inv} \left(V_G - V_T - \frac{V_D}{2} \right) \quad (1.1)$$

where W is the width of the transistor channel, L is the channel length, μ is the channel carrier mobility, C_{inv} is the capacitance density associated with the gate dielectric when the underlying channel is in the inverted state, V_G and V_D are the voltages applied to the transistor gate and drain, respectively, and the threshold voltage is given by V_T . It can be seen that in this approximation the drain current is proportional to the average charge across the channel (with a potential $\frac{V_D}{2}$) and the average electric field $\left(\frac{V_D}{L}\right)$ (along the channel direction). Inertially, I_D increases linearly with V_D and then eventually saturates to a maximum when $V_{D,sat} = V_G - V_T$ to yield

$$I_{D,sat} = \frac{W}{L} \mu C_{inv} \left(\frac{V_G - V_T}{2} \right)^2 \quad (1.2)$$

There are several possible ways of improving $I_{D,sat}$.

Decrease in channel length L

The reduction of the transistor channel length is driven by the need of decreasing chip area on the Si wafer and thus decreasing the chip cost. The physical channel

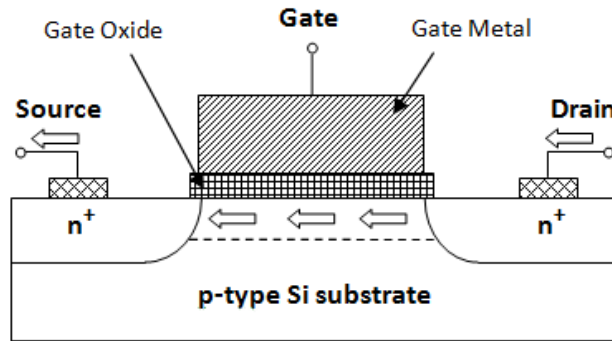


Figure 1.1: Schematic cross-section of the traditional MOSFET transistor

length continues to scale by a factor 0.7 per technology generation, thus doubling the transistor density [3]. According to Eq. (1.2), the scaling down of the channel length provides also a significant improvement in the drive current.

Increase in gate overdrive ($V_G - V_T$)

The term $(V_G - V_T)$ is limited in range due to reliability and room temperature operation constraints, since too large a V_G would create an undesirable, high electric field across the oxide. Furthermore, V_T cannot easily be reduced below about $200mV$, because $kT \sim 25mV$ at room temperature. Typical specification temperatures ($< 100^\circ C$) could therefore cause statistical fluctuations in thermal energy, which would adversely affect the desired V_T value.

Increase in channel carrier mobility μ

A significant improvement of the carrier mobility can be indeed achieved by the implementation of new MOSFET channel materials (most notably, strained silicon and germanium) [4, 5]. This approach is considered to be the key in providing performance boost required for the next MOSFET generation.

Increase in channel width W

An increase in the channel width, without increasing chip area, implies severe changes in device architecture. Transition from the conventional planar MOSFETs to three-dimensional (3-D) structures, such as double-gate MOSFETs [6] would provide a large performance gain and an ideal structure for scalability. However, a manufacturable realization of such 3-D architecture by using conventional planar production processes presents a formidable challenge. Very promising solutions are the FinFET (Fin Field Effect Transistor) and ITFET (Inverted T channel Field Effect Transistor) architectures [7] [8] [9], which could eventually enable the production of double-gate MOSFETs in CMOS technology.

Increase in gate capacitance C_{gate}

In the case of increasing the gate capacitance, consider a parallel plate capacitor (ignoring quantum mechanical and depletion effects from a Si substrate and gate)

[10]

$$C_{gate} = \frac{k\epsilon_0 A}{t} \quad (1.3)$$

where k is the dielectric constant (also referred to as the relative permittivity in this article) of the material, ϵ_0 is the permittivity of free space, A is the area of the capacitor, and t is the thickness of the dielectric. For device design, all FET dimensions scale proportionately and the precise material does not affect electrical designs, so it is convenient to define an "electrical thickness" of the new gate oxide in terms of its equivalent silicon dioxide thickness or "equivalent oxide thickness" (EOT) as

$$t_{ox} = EOT = \frac{3.9}{k} t_{high-k} \quad (1.4)$$

Here 3.9 is the static dielectric constant of SiO₂. The objective is to develop high K oxides which allow scaling to continue to ever lower values of EOT.

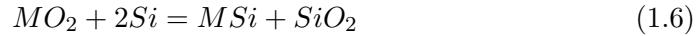
1.2 High-k gate dielectric

Silicon dioxide is the key reason that microelectronics technology uses Si and not some other semiconductor. Si is an average semiconductor in performance, but in all other aspects SiO₂ is an excellent insulator. SiO₂ has the key advantage that it can be made from Si by thermal oxidation, whereas every other semiconductor (Ge, GaAs, GaN, SiC...) has a poor native oxide. SiO₂ is amorphous, has very few electronic defects and forms an excellent interface with Si. It can be etched and patterned to a nanometer scale. Its only problem is that when very thin it is possible to tunnel across it. Hence, we must lose these advantages of SiO₂ and start to use a new high-k oxide. We can in principle choose from a large part of the Periodic table:

- It must have a high enough K that it will be used for a reasonable number of years of scaling.
- The oxide is in direct contact with the Si channel, so it must be thermodynamically stable with it.
- It must be kinetically stable, and be compatible with processing to 1000°C for 5 seconds.
- It must act as an insulator, by having band offsets with Si of over 1 eV to minimise carrier injection into its bands.
- It must form a good electrical interface with Si.
- It must have few bulk electrically active defects.

Selecting a gate dielectric with a permittivity higher than that of SiO₂ is clearly essential. K should be over 10, preferably 25-30. In fact, a huge K is undesirable in CMOS design because they cause undesirably strong fringing fields at source and drain electrodes [11]. The high K oxide must act as an insulator. This requires that the potential barrier should be large enough to limit leakage current. For electrons and holes traveling from the silicon substrate to the gate, this barrier is the conduction band offset, ΔE_c and the valence band offset, ΔE_v respectively. A gate dielectric must have a sufficient both ΔE_c and ΔE_v to poly-Si (must be over 1 eV), and to other gate materials in order to inhibit conduction by the Schottky emission of electrons and holes to the oxide bands. These limits the choice of oxide to those with band gaps over 5 eV. The oxides that satisfy this criterion are Al₂O₃, ZrO₂, Y₂O₃, La₂O₃ and HfO₂ [12]. Hf-oxide has enough large dielectric constant about 20 and relatively wide band 5.6eV together with more than 1eV offsets for both conduction and valence bands.

For all thin gate dielectrics, the interface with silicon plays a key role, and in most cases is the dominant factor in determining the overall electrical properties. The oxide must not react with Si to form either SiO₂ or a silicide according to the unbalanced reactions,



This is because the resulting SiO₂ layer would increase the EOT and negate the effect of using the new oxide. In addition, any silicide formed by 1.6 would generally be metallic and would short out the field effect. This effect can be understood by noting that, when the structure contains several dielectrics in series, the lowest capacitance layer will dominate the overall capacitance, setting in this way a limit on the minimum achievable t_{eq} value. The total capacitance C_{total} of dielectric stack composed of two layers, a low- k and high- k layer, with capacitance C_1 and C_2 , respectively, is given by

$$\frac{1}{C_{total}} = \frac{1}{C_1} + \frac{1}{C_2} \quad (1.7)$$

Hence, t_{eq} of the dielectric stack

$$t_{eq} = \frac{\epsilon_{SiO_2}}{\epsilon_{low-k}} t_{low-k} + \frac{\epsilon_{SiO_2}}{\epsilon_{high-k}} t_{high-k} \quad (1.8)$$

It is clear from 1.8 that minimum achievable oxide thickness is limited by that of the lower- k layer. This condition requires that the oxide has a higher heat of formation than SiO₂. Hubbard and Schlom [13, 14] found that this restricts the possible oxides to very few, from columns II, III and IV of the Periodic table. These

are SrO, CaO, BaO, Al₂O₃, ZrO₂, Y₂O₃, La₂O₃ and HfO₂. It excludes some otherwise useful and familiar oxides such as Ta₂O₅, TiO₂ and the titanates including SrTiO₃ and BaTiO₃, which were favoured for use in capacitors in DRAMs. The group II oxides SrO, etc. are not favoured of themselves because they are very reactive with water. However, they would be acceptable as a transition layer. Hence this leaves us Al₂O₃, ZrO₂, Y₂O₃, La₂O₃, HfO₂ and various lanthanides such as Pr₂O₃, Gd₂O₃ and Lu₂O₃. Zr and Hf are both from column IV and are generally believed to be the two most similar elements in the main Periodic table. However, it also turns out that the thermodynamic data for many oxides were not so accurate. It was subsequently found that ZrO₂ is actually slightly unstable [15, 16] and can react with Si to form the silicide, ZrSi₂. For this reason, HfO₂ is presently the preferred high-k oxide over ZrO₂. La₂O₃ has a slightly higher K than HfO₂, but is more hygroscopic. Al₂O₃ has the disadvantage of a rather low K value. Y₂O₃ also has a lower K than La₂O₃. The other lanthanides Pr₂O₃, Gd₂O₃ and Lu₂O₃ are comparable to La [17, 18, 19, 20]. Alternatively, the superior SiO₂/Si interface characteristics leads one to consider a thin SiO₂ layer coupled with a high-k dielectric to avoid degradation of the carrier mobility in the transistor channel.

The oxide is in direct contact with the Si channel. The carriers induced by the gate are induced within Angstroms of the Si-oxide interface. Hence, this interface must be of the highest electrical quality, in terms of roughness and the absence of interface defects. It is difficult to imagine any material creating a better interface to Si than that of SiO₂, since typical industrial SiO₂ gate dielectrics have a low midgap interface state density, D_{it} , of $\sim 2 \times 10^{10}$ states/cm²eV. Most high-k material reported show D_{it} values of $\sim 10^{11} - 10^{12}$ states/cm²eV. Extra defects are associated with oxide grain boundaries. Therefore, there are two ways to ensure a high quality interface, either use a crystalline oxide grown epitaxially on the Si, or use an amorphous oxide. Using an amorphous oxide has many advantages over a poly-crystalline oxide. It is like the existing Si:SiO₂ situation. Using an amorphous oxide has many advantages over a poly-crystalline oxide. First, an amorphous oxide might be able to configure its interface bonding to minimize the number of interface defects. Second, it is possible to gradually vary the composition of an amorphous oxide without creating a new phase; for example as in silicate alloys, or interfacial layers, or when adding nitrogen. Third, an amorphous oxide and its dielectric constant is isotropic, so that fluctuations in polarization from differently oriented oxide grains will not scatter carriers. Finally, amorphous phases have no grain boundaries. Grain boundaries in a polycrystalline oxide act as easy diffusion paths for dopants, such as B or P from a poly-Si gate electrode lying above. The advantages of epitaxial oxides may come in the future, where their ability to create more abrupt interfaces allows us to reach lower EOTs. Electrically active defects are defined as atomic configurations which give rise to electronic states in the band gap of the oxide. Typically these are sites of excess or deficit of oxygen or impurities. Defects are undesirable for four reasons.

Firstly, charge trapped in defects causes a shift in the gate threshold voltage of the transistor, the voltage at which it turns on. Secondly, the trapped charge will change with time so the threshold voltage will shift with time, leading to instability of operating characteristics. Thirdly, trapped charge scatters carriers in the channel and lowers the carrier mobility. Fourthly, defects cause unreliability; they are the starting point for electrical failure and breakdown of the oxide. SiO_2 is an almost ideal insulating oxide, in that it has a low concentration of defects which give rise to states in the gap. This is fundamentally because it has a low coordination number, so that its bonding can relax and rebond any broken bonds at possible defect sites. Any remaining defects are passivated by hydrogen. The high-k oxides are not materials with a low intrinsic defect concentration because their bonding cannot relax as easily. Much of the present-day engineering of these oxides consists of pragmatic strategies of trying to reduce defect densities by processing control and annealing. The great advantage of SiO_2 is that it can be grown by thermal oxidation. In contrast, high-k oxides must be deposited. Deposited oxides are never as good. A crucial factor in determining high-k dielectric final film quality and properties is the choice of the deposition process. It must be compatible with current or expected CMOS processes, cost and throughput. It is therefore important to consider various manufacturable methods such as physical vapor deposition (PVD), chemical vapor deposition (CVD) and atomic layer deposition (ALD). PVD methods have provided convenient mean to evaluate alternative dielectric materials. However, PVD's inherent surface damage results in unwanted interface states. Additionally, device morphology inherent to sub micron scaling generally rules out such line-of-sight PVD approaches. For this reasons, CVD and ALD methods are preferred. CVD uses a volatile metal compound as a precursor which is introduced into the chamber and oxidized during deposition onto the substrate. The advantages of CVD are that it is already widely used in the electronics industry for insulator deposition, it gives conformal coverage over complex shapes because it is not just line of sight, and that the growth rate is controllable over a wide range from very slow to high. Atomic layer deposition is a method of cyclic deposition and oxidation, where metallic precursor and oxidation pulses are separated by inert gas purge [21]. The advantages of ALD are that it is able to grow the thinnest films of all methods, and the most conformal films even into deep trenches. A disadvantages are its slow growth rate and that they generally introduce impurities into the oxides, such as C, H or Cl, depending on precursor, whose electrical activity needs careful study. Careful annealing strategies are needed to densify the CVD and ALD oxides and remove impurities. This and other reasons led to the adoption of ALD for many high-k oxides.

1.3 In-situ approach of investigation high-k oxide

The high-k oxide HfO_2 has a large dielectric constant of about 20, a large band gap of about 5.6 eV, and a band offset with Si of at least 1.5 eV on both valence and conduction band sides [22]. Its electrical properties are well known, as it is already in use as a substitute gate oxide for the Si-oxinitride in 45 nm silicon technology, and it will be certainly present in the next generation sub-32-nm nodes silicon technology [23]. Anyway, a better understanding of the influence of the growth procedure on the final electrical properties is a stringent condition for its wide spread application [24, 25]. The ALD growth of HfO_2 has been extensively investigated in the last years gaining an in-depth knowledge of its properties [26, 27] with the past studies focused mainly on the setting of the parameters for obtaining good quality films. In particular, the choice of the Hf and O precursors and the determination of the ideal substrate temperature have been considered. However, a more detailed knowledge of every single step constituting each ALD cycle is to be gained, in order to clarify behaviors that are still an issue in the ALD growth [28]. Among the most important issues to be solved is the formation of an interracial layer with poor dielectric properties that increases the equivalent oxide thickness EOT. This consideration concerns especially the early stages of the film growth and the interface formation with the Si substrate. A few works, experimental and theoretical, were devoted to the detailed investigation of the initial growth of HfO_2 [28, 29, 30, 31] coming to the conclusion that the "growth per cycle" is not constant during the growth of the very initial layers because the ALD process changes the characteristics of the substrate while depositing new material. The experimental investigations were made ex-situ. Thin films, prepared with a certain number of cycles, were moved into the measurement chamber and analyzed by means of atomic force microscopy, Rutherford backscattering spectroscopy and x-ray photoelectron spectroscopy (XPS), and electrically characterized. Based on those experimental observations, Alam and Green [30] and Puurunen [32] proposed two different models for describing the initial growth of HfO_2 on various substrates, using HfCl_4 as Hf precursor. However, the ex-situ approach may suffer of two types of experimental problems, which may influence the final result. The possible exposure to ambient contaminations during the transfer into the measurement chamber may induce changes in the properties of the sample, such as the growth of an interfacial layer [33]. The measurements, made after a certain number of cycles, may miss the detailed information of the single cycles and provide an average approximation of the total effects of the performed cycles. To overcome the issue of sample contamination, some groups have implemented in-situ experiments and have investigated the initial growth of HfO_2 and Al_2O_3 on Si by means of optical spectroscopy [34], x-ray reflectometry XRR, x-ray fluorescence XRF [35], XPS [36] and reflection high-energy electron diffraction [37]. Here we propose an in-situ study of the ALD growth of HfO_2 using a reactor attached to the measurement chamber kept at UHV conditions and equipped with an electron analyzer for recording photoemission and x-ray absorp-

tion spectroscopy XAS spectra. In this way, we could transfer the freshly prepared film into the measurement chamber without breaking the vacuum and avoiding any possible contamination. With the in-situ equipment, we could control the quality and the property of the substrate before the ALD deposition by characterizing the clean sample with photoemission and XAS and then studying the sample after each cycle. Moreover, we could take advantage of the high resolution of synchrotron radiation SR that permits photoemission measurements with very high sensitivity. The possibility to tune the photon energy in a wide range allowed recording alternatively surface or bulk sensitive XPS spectra and measuring XAS spectra, thus providing important information about the atomic composition and the chemistry of the oxide. The possibility to measure at very surface sensitive conditions is very important when considering that the EOT of the next generation processors needs to be below 1 nm. In that case, the formation of an interfacial layer of the order of 1 nm should be clearly detectable in order to study it appropriately.

Chapter 2

Basics

2.1 Atomic Layer Deposition

The ALD technology was developed and patented some 30 years ago by Suntola and co-workers in Finland [38]. The purpose was to develop TFEL displays where ALD, then known as ALE, was used to deposit the high quality electroluminescent and dielectric layers, the latter being closely related to the high-k dielectrics. The TFEL display production was the first industrial application of ALD and the successful industrial production still continues. The strength of the ALD technology lies in its capability to produce high-quality, dense, and pinhole-free films on large surface areas with excellent uniformity and conformality as well as with thickness and composition control at an atomic level [39]. These characteristics are now especially needed for the processing of high-k dielectrics. The ALD processes and their applications have been frequently reviewed [39, 40, 41, 42, 43], most extensively and recently by Puurunen [44]. ALD is a variant of chemical vapor deposition (CVD) method, but unlike CVD, ALD relies on sequential and saturating surface reactions of the alternately applied precursor pulses. The precursor pulses are separated by inert gas purging or evacuation of the reaction chamber to avoid gas phase reactions between the precursors. The growth proceeds in a cyclic manner enabling easy thickness control. The basic principle of ALD is shown in a simplified manner in Figure 2.1, where one ALD cycle of an imaginary metal oxide deposition is presented. At first the exposure of the substrate surface to the gaseous metal precursor (a) and its chemisorption on the available surface sites (here OH groups) leaves the surface saturated. After inert gas purging of the excess precursor and ligand exchange by-products (b), the surface is exposed to the oxygen source (here H₂O) (c). The surface reaction produces the desired oxide film and after inert gas purging the surface is ready for the next ALD cycle (d). In order to achieve a surface saturative ALD-type process, the growth rate has to be independent of the precursor dose provided that

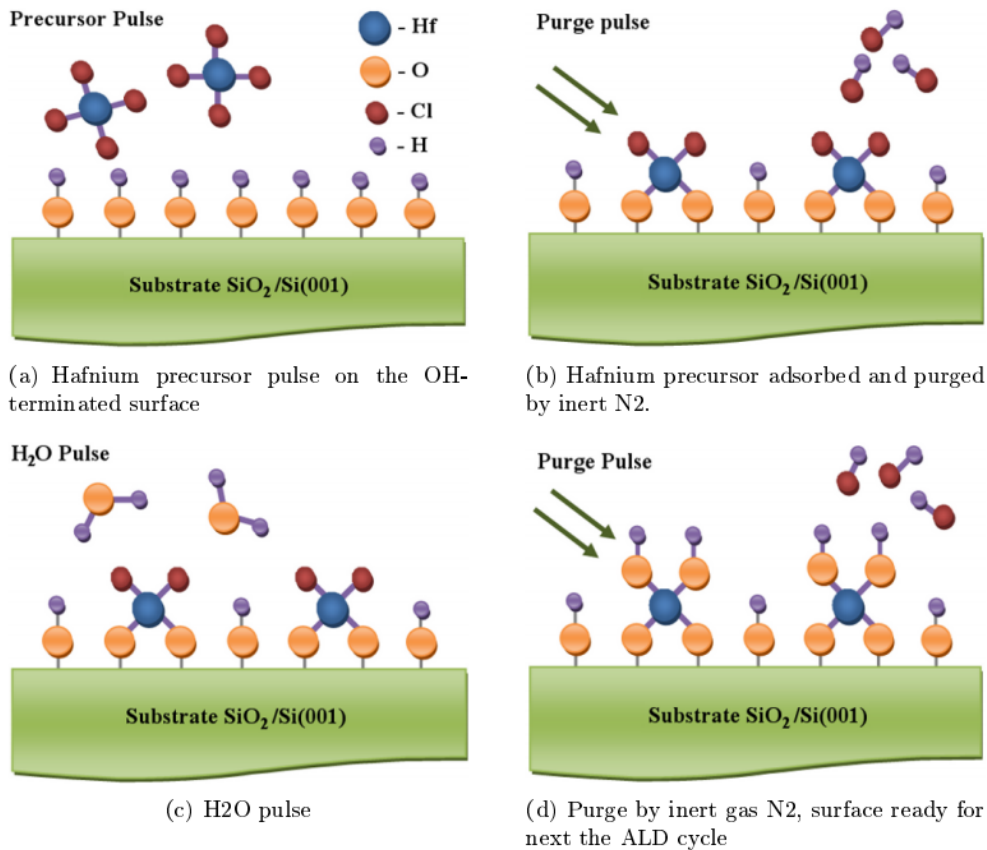


Figure 2.1: Schematic illustration of an ALD cycle of a Hf-oxide process where HfCl₄ precursors and H₂O are alternately pulsed and separated by inert N₂ gas pulsing

the dose is sufficiently large so that all the available surface sites have been occupied (Figure 2.2). In other words, the precursor decomposition leading to a CVD-type growth mode should be avoided. In theory, the ALD growth proceeds by one atomic layer per cycle, but in practice, due to steric hindrances and possible limited number of reactive surface sites, the growth rate per cycle usually is only a distinct fraction of a monolayer (ML) thickness, typically less than 0.5 ML. As the growth proceeds in a cyclic manner, and the purging periods take some time, the ALD technique is rather slow for some applications, but for high-*k* depositions where very thin films are grown this is not a critical issue. Often, but not always, a region with a constant deposition rate, also known as ALD window, is observed [40, 45]. The ALD window is not a requirement for an ALD-type growth mode, but it is a desirable feature that leads to the reproducibility of the film growth. Especially if a ternary material is to be deposited, overlapping ALD windows of the constituent binary processes offer a good starting point for the development of a ternary process. The observed growth rates vs. temperature in ALD processes are shown in Figure 2.3. In addition to

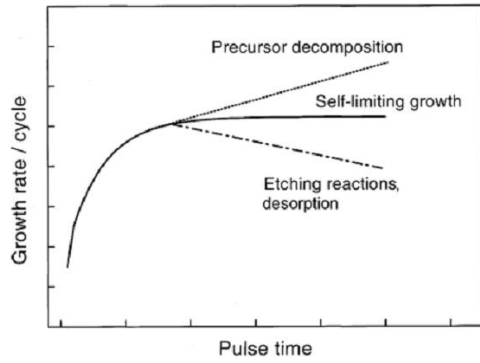


Figure 2.2: Different types of growth rate vs. precursor pulse time curves in ALD processes at a constant temperature

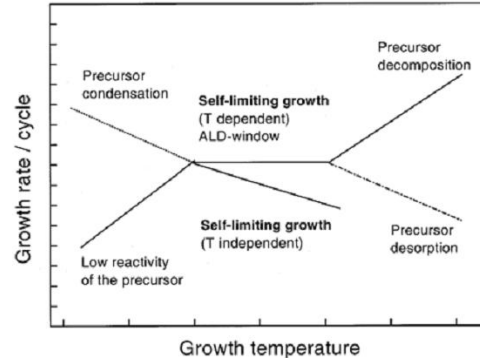


Figure 2.3: Factors limiting the self-limiting growth at various temperatures

the above-mentioned applications in microelectronics, ALD certainly offers potential solutions in many other areas, such as optics and optoelectronics, nanotechnology, micro-electromechanical systems, catalysis, magnetic recording head technology, and protective and antireflective coatings.

2.2 X-ray Photoelectron Spectroscopy

X-ray photoelectron spectroscopy (XPS) is a quantitative spectroscopic technique that measures the elemental composition, empirical formula, chemical state and electronic state of the elements that exist within a material. XPS spectra are obtained by irradiating a material with a beam of X-rays ($MgK\alpha$, $AlK\alpha$ or Synchrotron Radiation) while simultaneously measuring the kinetic energy (KE) and number of electrons that escape from the top 1 to 10 nm of the material being analyzed. The emitted electrons have kinetic energies given by

$$E_{kin} = h\nu - E_{bind} - \Phi_{spec} \quad (2.1)$$

where $h\nu$ is energy of photon, E_{bind} is the binding energy of atomic the orbital from which the electron originates, and Φ_{spec} is work function of spectrometer. Process of electron excitation and analyzing are shown on Fig. 2.4. Because each element has unique binding energies, XPS can be used to identify and determine concentration of the elements in the surface. Variation the elemental binding energies (the chemical shift) arise from the differences in the chemical potential and compound polarizability. These chemical shift can be used to identify the chemical state of material being analyzed. For the most XPS investigation, quantitative analysis is important. Using area peak intensity we can determine the relative concentrations of various constituents, depth profiling and the thickness of one or more thin layers.

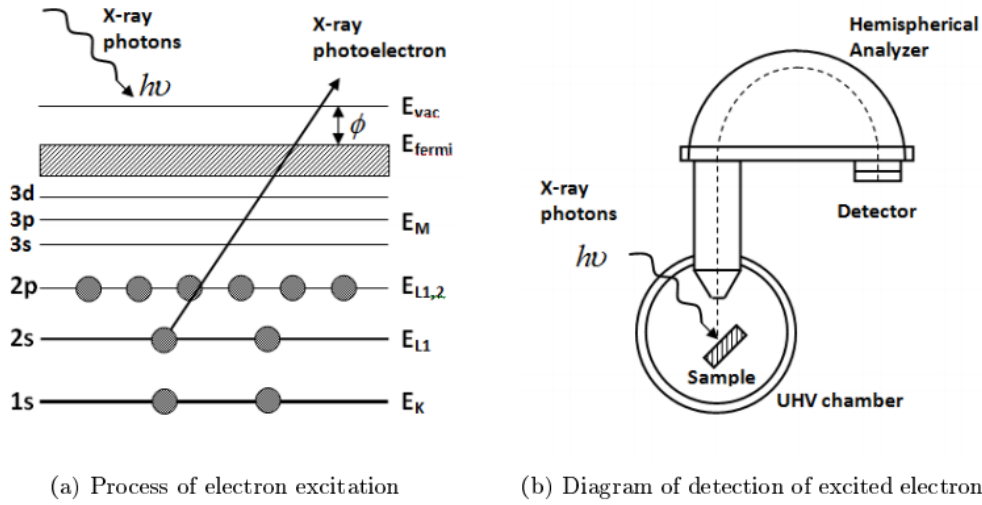


Figure 2.4: Schematic illustration of an XPS experiment with excitation of electrons and following their analyzing and detection

Total area peak intensity depends on many factors. We can separate these factors for two groups. The first group depends on experimental instruments (X-ray source, type of analyzer, experimental geometry and etc.). The second one comes from physical properties of investigated sample. For the simple case (Fig. 2.5) intensity from element A can be estimated by equation:

$$I_A = f\beta N_A \sigma_A T(E_A) \int_{x_1}^{x_2} \exp\left(-\frac{z}{\lambda_A \cos \theta}\right) dz \quad (2.2)$$

where f is photonflux of used x-ray source, β is an angular efficiency factor for the instrumental arrangement based on angle between the photon path and detected electron, $N = N_0 \rho / M$ is the atomic density (N_0 is Avogadros constant, ρ is the density of the sample and M is the relative atomic mass), σ is the ionization cross-section of the observed photoelectron line according to a defined core level and the photonenergy $h\nu$, λ is the inelastic mean free path and $T(E)$ - is the transmission function of the spectrometer used. If we have infinitely thick layer with homogeneous distributed atoms A, intensity from these atoms is given by

$$I_A = f\beta N_A \sigma_A T(E_A) \lambda_A \cos \theta \quad (2.3)$$

For a sample consisting of a thin homogeneous layer of material B with thickness d on a substrate of material A (Fig. 2.6), we can write the following expressions for the XPS signal intensities assuming exponential attenuation in the overlayer:

$$\frac{I_B}{I_A} = \frac{N_B \sigma_B T(E_B) \lambda_{B,B} (1 - \exp(-d/\lambda_{B,B}))}{N_A \sigma_A T(E_A) \lambda_{A,A} \exp(-d/\lambda_{B,A} \cos \theta)} \quad (2.4)$$

where $\lambda_{B,B}$ and $\lambda_{A,B}$ are the attenuation lengths in the overlayer of photoelectrons emitted from the overlayer and the substrate, respectively. The $\lambda_{A,A}$ is attenuation

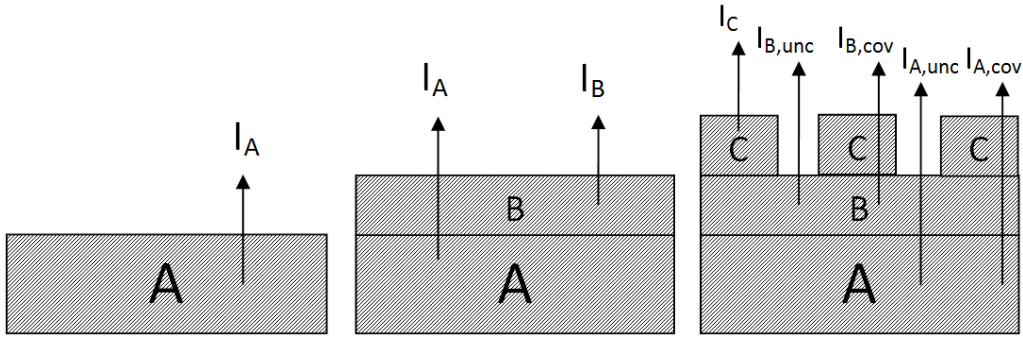


Figure 2.5: Sample structure. Infinitely thick homogeneous sample

Figure 2.6: Sample structure. The sample consisting of a thin homogeneous layer on substrate

Figure 2.7: Sample structure. The sample consisting of a thin island layer on substrate

lengths of substrate electrons in the substrate. The last equation 2.4 can be used for thickness calculation of SiO_2 layer on top of Si. For this case the kinetic energy of Si2p photoelectrons from oxidized and elemental Si differ by less than 4eV (0.3%) $\lambda_{B,B} = \lambda_{A,B} = \lambda$

$$d = \lambda \cos \theta \ln\left(1 - K \frac{I_B}{I_A}\right) \quad (2.5)$$

where $K = \frac{N_A \sigma_A \lambda_{A,A}}{N_B \sigma_B \lambda_{B,B}}$ In-situ experiment give possibility to measure signal of substrate before deposition of overlayer. Using information about attenuation of substrate signal in the deposited overlayer we can calculate thickness:

$$d = \lambda \cos \theta \ln\left(\frac{I_0}{I}\right) \quad (2.6)$$

where I_0 and I are intensities of signal before and after deposition respectively. All above equations are corrected for homogeneous layers only. Studying of the initial ALD cycles we have to do with islands of capped layer. The structure of the sample with islands of top layer is demonstrated on figure 2.7. The signals from the bottom layers consist of two contributions. One is covered and attenuated by top layer. The second one is uncovered. The signals from all three layers can be described by equations:

$$I_C = F * N_C \lambda_{C,C} \sigma_A T(E_C) \cos \theta (1 - \exp(-d_C / \lambda_{C,C} \cos \theta)) \quad (2.7)$$

$$I_{B,cov} = F * N_B \lambda_{B,B} \sigma_A T(E_B) \cos \theta (1 - \exp(-\frac{d_B}{\lambda_{B,B} \cos \theta})) \exp(\frac{d_C}{\lambda_{B,C} \cos \theta}) \quad (2.8)$$

$$I_{B,unc} = (1 - F) * N_B \lambda_{B,B} \sigma_A T(E_B) \cos \theta (1 - \exp(-\frac{d_B}{\lambda_{B,B} \cos \theta})) \quad (2.9)$$

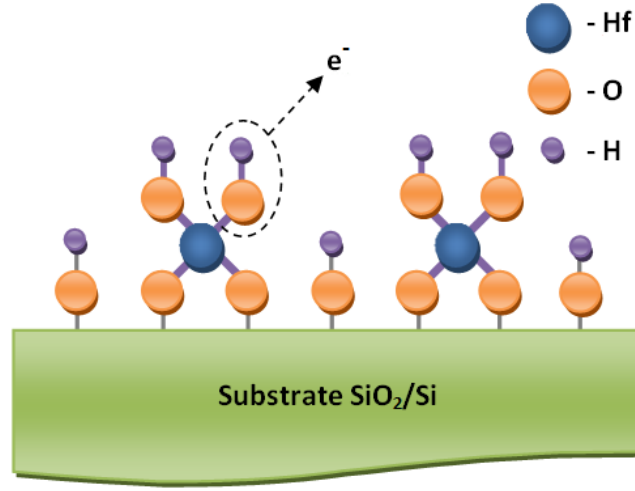


Figure 2.8: Absorption geometry of HfO₂ molecules on SiO₂/Si substrate

$$I_{A,cov} = F * N_A \lambda_{A,A} \sigma_A T(E_A) \cos \theta \exp\left(\frac{d_B}{\lambda_{A,B} \cos \theta}\right) \exp\left(\frac{d_C}{\lambda_{A,C} \cos \theta}\right) \quad (2.10)$$

$$I_{A,unc} = (1 - F) * N_A \lambda_{A,A} \sigma_A T(E_A) \cos \theta \exp\left(\frac{d_B}{\lambda_{A,B} \cos \theta}\right) \quad (2.11)$$

where F is the coverage of islands, $\lambda_{A,A}$, $\lambda_{A,B}$ and $\lambda_{A,C}$ are attenuation length of substrate electrons in the substrate A , intermediate layer B and islands C , respectively, $\lambda_{B,B}$ and $\lambda_{B,C}$ are attenuation length of intermediate layer electrons in the intermediate layer B and islands C , respectively, $\lambda_{A,A}$ is attenuation length of electrons from island in the island C . In the experiment we have three signals: I_C is due to islands of material C , $I_B = I_{B,cov} + I_{B,unc}$ is the sum of the signals from the intermediate layer and $I_A = I_{A,cov} + I_{A,unc}$ is the total substrate signal. Operating with these data we can estimate the thickness of all layers, their stoichiometry and the coverage, follow the evolution of HfO₂ growth and changes in the interfacial layer. When we analyze XPS data and calculate the physical parameters of the ultra thin layers (one or two monolayers) we should take to account the absorption geometry of molecules. One possible case is represented in Fig. 2.8. Oxygen atoms from HfO₂ molecules is on top and exciting electrons from these atoms are collected directly by analyzer without any attenuation. In thick layer we can neglect by this contribution, but for the film with monolayer thickness it is very important.

Chapter 3

Experimental

3.1 The ALD in-situ system

The ALD reactor comprehends a stainless-steel UHV-compatible vessel equipped with a turbo-molecular pump system, a pressure gauge, a heating finger, a manipulator and a Gas Delivery System (GDS). The GDS is mounted on a 63mm flange and is formed by industrial graded electro-polished with various gas lines (Fig. 3.1). We developed two configurations for the gas delivery: a first one is made by one metal-precursor source, one oxygen source and one purging gas. In this configuration the purging gas can be delivered directly into the ALD reactor or may be deviated into the metal-precursor line for using it as carrier gas. In the second configuration there could be used two different metal-precursors, as each line is connected with a remote purging gas source. As in the first configuration, the third line is used for delivering the oxygen source. Every source is separated by fast pneumatic membrane-valves (Swagelok Diaphragm Valves), assuring a fast opening/closing time and good leak. The pumping system consists of a rotary vane pump for pumping the system from atmospheric pressure and a turbo-molecular pump assuring a base pressure in the 10^{-8} mBar range. The pumping speed of the turbo-molecular pump makes it possible to remove the excess gases and the byproducts of the ALD reactions in a fast and effective way. The pressure behavior during a usual ALD cycle we can see in Fig. 3.2. When opening the valve to the metal precursor the pressure rapidly increases reaching a pressure of 10^{-5} - 10^{-3} mBar, depending on the precursor used. The usual opening time is between 0.3s and 4s, also depending on the precursor used. To reduce the condensation of the metal precursors on the walls of either the UHV chamber or the GDS, both can be heated through heater tapes at temperatures varying between 50°C and 130°C. Between the pulses of the metal precursor and water, all the GDS and the UHV chamber are purged by introducing the inert gas to a pressure as high as 10^{-2} mBar. For further increasing the pumping speed efficiency, we perform a

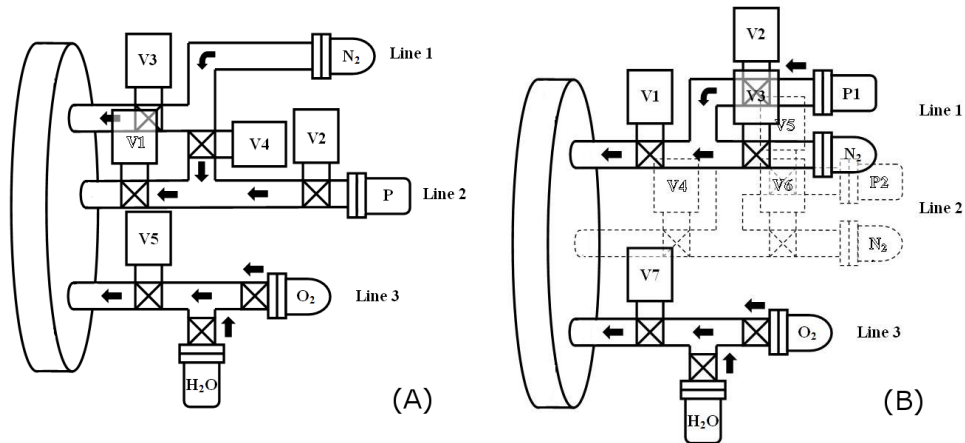


Figure 3.1: (A) The Gas Line System for ALD process with 3 lines: purging (line 1), precursor (line 2) and oxygen source (line 3) (B) The Gas Line System for ALD process for two precursors. The lines 1 and 2 are precursor source with independent purging gas. The line 3 is oxygen source. The black arrows show the direction of a gas flow.

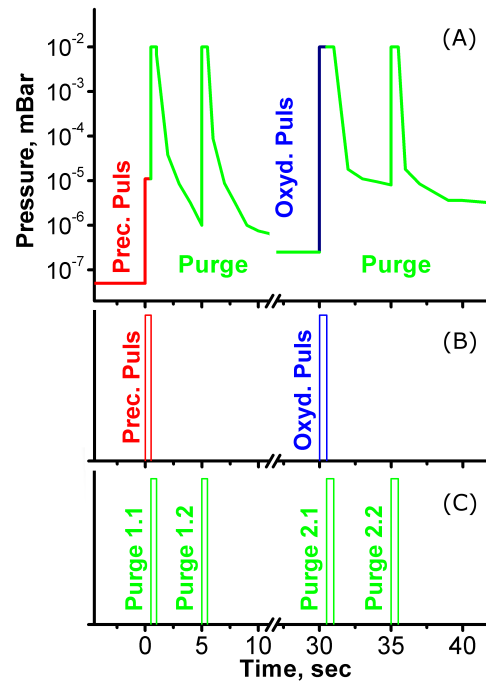


Figure 3.2: Pressure behavior in the ALD reactor during usual ALD cycle (A). Time of precursor, oxygen and purging pulses (B and C)

second purging pulse after 5 seconds. This further step assures that the complete GDS is completely evacuated. After this second purging step the pressure decreases steeply reaching a value around 5×10^{-7} mBar within 10s. After pumping out for 20 seconds the water pulse can be performed, being the pressure about 2×10^{-7} mBar. The water pulse is also usually about 0.3s-0.5s and brings the pressure in the UHV chamber up to 10^{-2} mBar. After the water pulse a two-step purge is performed. The pressure decrease after the water pulse and the purge is slower compared to the decrease after the metal precursor, as water may condensate easily on the UHV chamber even when it is heated (usually at 80°C). Anyway, after the complete cycle, the base pressure is restored within 2-3 minutes. The transfer into the UHV chamber for the measurements is done opening the valve separating the two vessels. The measurements chamber has a usual base pressure of about 2×10^{-10} mBar. This increases during the transfer, but it decreases again within some minute in the 10^{-10} mBar range, showing that the pressure increase is mostly due to the inert gas in the ALD reactor. The heating system is necessary as ALD needs a substrate temperature between 200°C and 400°C for growing amorphous metal oxides [46]. In this range the possible methods for heating the substrate are the direct heating (for semiconductor substrates) or the indirect one obtained either by radiative or contact heating. As the main experiments were done on Si substrates, we employed the resistive heating by applying a voltage between the two extremes of the Si sample. For obtaining similar temperature for each new sample and after each cycle we first calibrated the temperature dependency on the electrical power applied with both a thermocouple attached to the sample and an IR pyrometer with a large temperature spectrum. For this purpose we included a ZnSe window flange in the UHV reactor. The temperature accuracy is of the order of 10°C , but this does not preclude the reproducibility of the ALD cycles as the usual ALD windows have a typical range of at least $50\text{-}100^\circ\text{C}$. The software for controlling ALD valves was developed in our group using a NI LabVIEW Development System [47]. This software makes possible to control up to 8 valves in the system. It is possible to set the open/close time, the opening order, the number of cycles and the time between the cycles. The ALD valves are connected to the computer via a ADVANTECH 8-ch Relay and 8-ch Isolated DI USB Module 4761 [48]. The open/close status is changed by applying a voltage of 24V when the valves are connected to pressured air at 5 Bar.

3.2 In-situ XPS and XAS system at BESSY

UHV-compatible ALD reactor is attached to a chamber provided for XPS and XAS measurements at the beamline U49/2-PGM2 in BESSY II, Berlin, Germany (Fig. 3.3). The synchrotron light focused onto the $1 \times 1 \text{ cm}^2$ sample in a 45° incidence geometry [22]. The emitted electrons were collected in an angle-integrated mode with a 180° hemispherical energy analyzer SPECS PHOIBOS 150 positioned at an emission

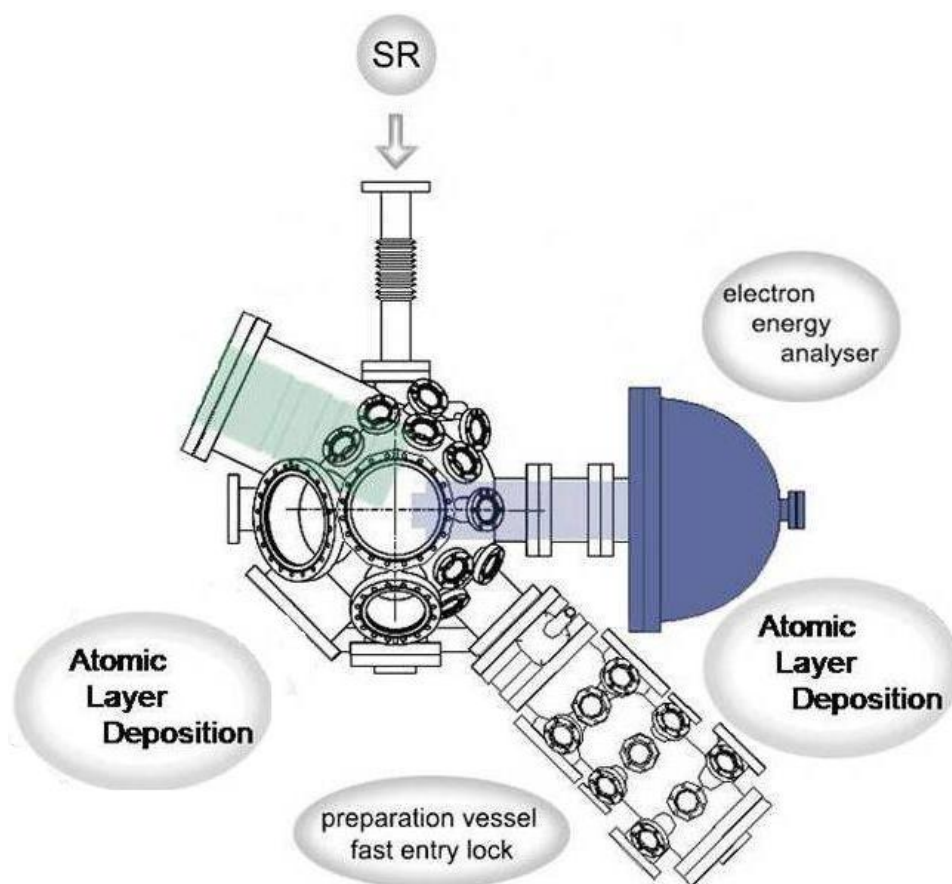


Figure 3.3: Diagram of in-situ XPS and XAS system with attached ALS reactor at BESSY

angle of 45° . The total energy resolution was set to about 100 meV for the spectra recorded at 150 eV, to 150 meV for the O1s, and to 200 meV for the Hf4d core level both measured at 600 (or 640) eV. The photon energy range of the U49/2 beam line in BESSY II is very large covering energies as low as 90 up to 1800 eV [23]. We have chosen the photon energies 150 and 600 (or 640) eV for the surface sensitive investigation of the Si2p and O1s core level peaks. The surface sensitivity was further increased by setting the emission angle to 45° . Thanks to these settings, we can show here very sensitive measurements that are not possible with the standard lab sources. The XAS spectra were recorded using both the total electron yield TEY, by measuring the drift current on the sample, and the partial electron yield, by measuring the intensity of the electrons with a kinetic energy of 50 eV with the electron analyzer.

3.3 Used Precursors

In our experiments we used three different precursors Hafnium tetrachloride, Tetra-(ethylmethylamino)hafnium and Tetrakis(dimethylamino)hafnium. They have various physical and growing ALD properties. Hafnium tetrachloride represents halides. It is a solid source material (powder) for the atomic layer deposition. In HfCl_4 molecular hafnium is bonded with four chlorine molecules. It has molecular weight is 320,30 g/mol. At room temperature HfCl_4 has too low vapor pressure (VP). Boiling point is 320°C . In our experiments the HfCl_4 precursor was heated up to 170°C . At this temperature pressure in ALD reactor changes from value 10^{-8} to 5.5×10^{-5} . The time of hafnium precursor pulse was 360 seconds. The optimized temperature of the substrate found in most studies is 300°C , showing well-saturated growth with a growth rate of 0.5-1.0 /cycle, the exact value depending on the reactor set-up. Hydrogen and chlorine impurity levels at 300°C have been reported to be 0.6-0.8 and 1.5 at-%, respectively [49]. The chlorine level could be reduced by annealing at high ($900\text{-}1050^\circ\text{C}$) temperatures [50]. However, annealing caused crystallization even in very thin layers [51]. The chlorine residues tend to accumulate at the interface region between the film and Si substrate [52]. Problems related to the $\text{HfCl}_4/\text{H}_2\text{O}$ process include also the fact that the metal precursor, being a fine solid, can generate particle contamination and the ALD reaction by-product is corrosive acid HCl [53]. In addition, the inhibited growth of hafnia on H-terminated Si, leading to an island-type growth [54, 55] remains as a challenge. A common solution to overcome this problem is to use thin thermal or chemical SiO_2 as a starting layer. However, as lower-k interfacial layer is introduced, to achieve sub-1.0 nm EOT values with low leakage becomes more difficult. For these obvious reasons alternative chemistries for the ALD of HfO_2 has been the subject of many researches. One possible candidates is alkylamides. TEMAHf is used essentially for the deposition of pure HfO_2 . It can be used both in ALD or MOCVD mode for the deposition of high-k films, with O_2 , O_3 and H_2O being the most common co-reactants. TEMAHf is a clear liquid that reacts immediately upon contact with water or moisture, with the evolution of ethylmethylamine and hafnium oxide/hydroxide formation. TEMAHf has an increased volatility and does not suffer from being a solid at room temperature. TDMAHf is solid at RT and becomes liquid at 60°C . A distinct benefit of using Hf alkylamides, TEMAHf and TDMAHf, is that they are liquid at the evaporation temperature eliminating the particle contamination problem [18]. Furthermore, the alkylamides are reactive towards water and give impurity levels that are at least for C and N reasonably low, e.g. 0.3-0.6 at-% of C and 2-3 at-% of H when $\text{Hf}(\text{NEtMe})_4/\text{H}_2\text{O}$ ALD-process was applied at 250°C [56]. The suitable ALD growth temperature range for the $\text{Hf}(\text{NEtMe})_4/\text{H}_2\text{O}$ process is reported to be below 350°C [18] but slight decomposition of the precursor was probably affecting the growth rate already at temperatures around 300°C [56]. As compared with TEMAHf, higher impurity levels were detected in films obtained from TDMAHf and water. In addition, the surface roughness increased rapidly at

	<i>Hafnium Tetra-chloride</i>	<i>TEMAHf</i>	<i>TDAMHf</i>
<i>Formula</i>	HfCl ₄	[(CH ₃)C ₂ H ₅)N] ₄ Hf	[(CH ₃) ₂ N] ₄ Hf
<i>Molecular Weight</i>	320.30 g/mol	410.90 g/mol	354.79 g/mol
<i>Substrate Temperature</i>	300°C	350°C	250°C
<i>Precursor Temperature</i>	170°C	RT	60°C
<i>Precursor Pulse</i>	10 ⁻⁵ mBar for 6 min	10 ⁻⁵ mBar for 4 sec	10 ⁻⁵ mBar for 1 sec
<i>Oxidation Pulse</i>	10 ⁻² mBar for 20 sec	10 ⁻² mBar for 1 sec	10 ⁻² mBar for 1 sec
<i>Purge Pulse</i>	10 ⁻² mBar for 120 sec	10 ⁻² mBar for 1 sec	10 ⁻² mBar for 1 sec
<i>Number of cycles</i>	8 cycles	20 cycles	12 cycles
<i>Measurements</i>	XPS: Si2p, O1s, Hf4d, VB XAS: O1s, Si2p	XPS: Si2p, O1s, Hf4d, VB XAS: O1s	XPS: Si2p, O1s, Hf4d, VB

Table 3.1: The parameters of the experiments with different precursors

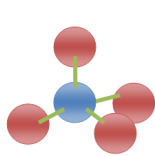
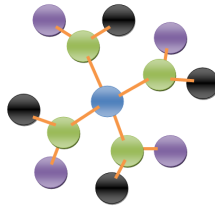
Figure 3.4: Molecular of HfCl₄

Figure 3.5: Molecular of TEMAHf

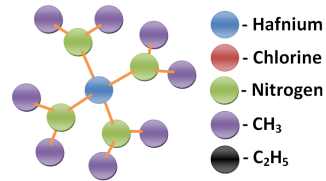


Figure 3.6: Molecular of TDMAHf

temperatures around 250°C [57]. All experimental parameters are collected in Tab 3.1.

Chapter 4

Results and discussion

4.1 Ex-situ investigation of industrial layers of Hf-oxide on Si by X-ray Photoelectron Spectroscopy

The ALD growth of hafnium oxide has been extensively investigated to obtain the best parameters of the ALD process to obtain good quality films. The most of experiments were carried out ex-situ. It means the investigated sample is exposed by an ambient influence, that can lead to undesirable additional contamination and reactions. As well as ex-situ measurements are made after certain number of ALD cycles and obtained information is an average approximation of the total effects of the performed cycles. In this section we want to demonstrate what kind information we can extract from ex-situ XPS spectra of industrial prepared Hf-oxide layers and show large disadvantages. In Fig. 4.1, 4.2 and 4.3 VB, O1s and Si2p spectra are collected. This sample was prepared by ALD and then ex-situ measured by XPS using SR. From experimental set-up we know that the sample is Si substrate p-type with SiO₂ and deposited 3nm overlayer of Hf-oxide, then sample was annealed. Ex-situ spectra give possibility to make qualitative analysis of the studied sample. Position and shape of spectra give information about chemical content. In Fig. 4.1 we show VB spectrum. The largest feature is Hf4f level peak at binding energy about 17.4eV indicating Hf content in the sample. Also we can observe two peaks at 25eV and lower 10eV due to oxygen atoms. In Fig. 4.2 O1s spectra are showed. It is one broad peak at 531.7eV and shoulder at lower BE about 530.7eV. The first peak comes from oxygen content in interface and indicate silicate formation. The second one is due to oxygen in Hf-oxide. Peak due to oxygen from SiO₂ is absent. In Fig. 4.3 you can see Si2p spectra. There are two features: one is signal from substrate at 98.7eV and second one comes from atoms of Si in the interface at about 102eV. The position of the second peak confirms the silicate formation in the interface. For the quantitative analysis we use the eq. 2.2. Actually we cannot use this equation directly, because

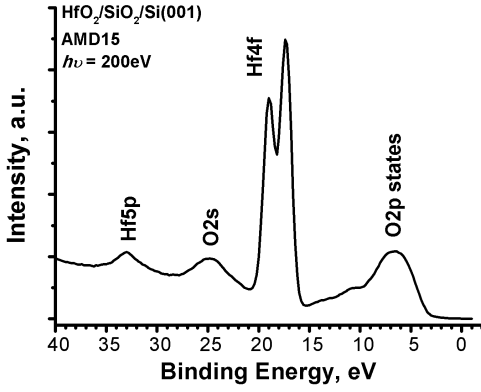


Figure 4.1: Ex-situ VB spectra for industrial Hf-oxide layer. The spectra were measured with photon energy of 200 eV. The major features of the VB and the core level lines are indicated.

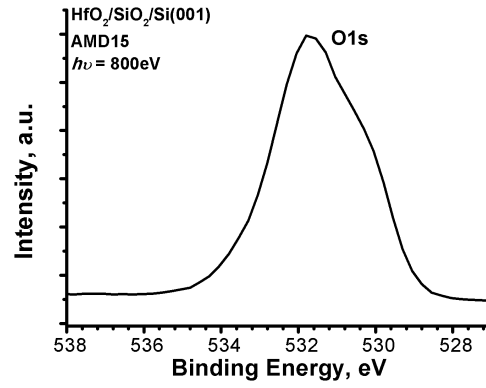


Figure 4.2: Ex-situ O1s spectra for industrial Hf-oxide layer. The spectra were measured with photon energy of 800 eV.

measured intensity is relative value and in analysis we should use relation between intensities of different core level peaks. Using 2.4 we can calculate thickness of IL. For SiO_2 or Silicate interface this equation does not depends on type and thickness overlayer, because kinetic energy of both excited electrons from the substrate and the interface is almost equivalent and these electrons are attenuated in the same way. From the calculation the thickness of IL is about 2.4nm. Now we come to large disadvantage of ex-situ experiment, because we don't know exactly initial conditions of substrate and cannot follow changes in the IL during and after deposition of Hf-oxide and after annealing. In contrast all this information can be obtained from in-situ experiment. To obtain information about structure of the sample should be used equation:

$$\frac{I_{\text{HfO}_2}}{I_{\text{Si}}} = K \frac{\lambda_{\text{HfO}_2, \text{HfO}_2} (1 - \exp(-d/\lambda_{\text{HfO}_2, \text{HfO}_2}))}{\lambda_{\text{Si}, \text{Si}} \exp(-d_{\text{HfO}_2}/\lambda_{\text{HfO}_2, \text{Si}} \cos \theta) \exp(-d_{\text{IL}}/\lambda_{\text{IL}, \text{Si}} \cos \theta)} \quad (4.1)$$

where K is $\frac{N_{\text{HfO}_2} \sigma_{\text{HfO}_2} T(E_{\text{HfO}_2})}{N_{\text{Si}} \sigma_{\text{Si}} T(E_{\text{Si}})}$. For ex-situ experiment this equation contains several uncertainties: the first one is thickness of the overlayer, the second one is changing of IL and the last one is stoichiometry of deposited layers. The first two parameters can be calculated from in-situ experiments using ratio between substrate signal and IL. Then stoichiometry can be estimated using Eq. 4.1. Ex-situ experiments give not enough information for complete analysis. Particularly when we deal with very thin films in-situ experiments are necessary. In following sections we will discuss advantages of in-situ XPS and XAS measurements.

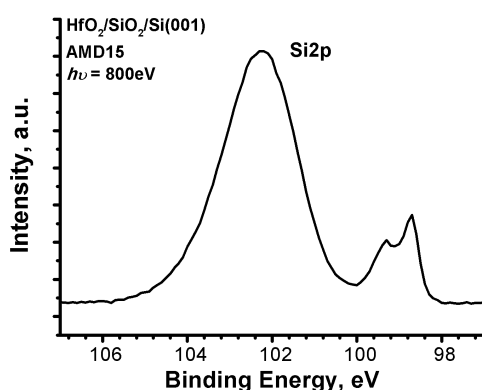


Figure 4.3: Ex-situ Si2p spectra for industrial Hf-oxide layer. The spectra were measured with photon energy of 800 eV.

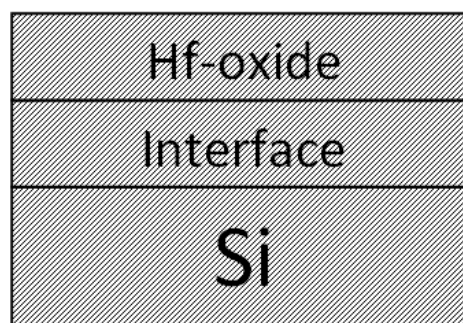


Figure 4.4: Structure of the ex-situ investigated sample.

4.2 Investigation of in-situ layers by XPS, XAS

4.2.1 Quantitative analysis

The high sensitivity of SR based electron spectroscopy is used to follow the intensities of the substrate signals as well as those of the hafnium oxide layers after each cycle. For the substrate, we use the Si2p core levels and the valence band (VB) spectra. The HfO₂ layer is characterized via the O1s emission, the Hf4f emission in the VB region, and for a better quantitative assignment also the Hf4d levels. Further information is obtained from the analysis of the XAS (only for the HfCl₄ experiment) spectra that were recorded at the Si2p edge and the O1s edge after each completed cycle. The intensities of all spectra shown here were divided by the incoming photon flux or the I₀ current measured by gold mesh, which are a function of time in a synchrotron.

In Fig. 4.5, 4.6, 4.7 and 4.8 we show the Si2p, VB, O1s and Hf4d variation for the etched substrate (blackline) and the complete ALD cycles. For the HfCl₄ experiments spectra are showed after each complete ALD cycle up to the seventh. For TDMAHf experiment we show spectra for substrate and after each two complete ALD cycles up to the twelfth. In Fig. 4.5 Si2p spectra are showed. The photon energy used for these spectra was 150 eV. The resolution for these spectra was set to about 100 meV, giving the possibility to observe the spin-orbit splitting (about 0.61 eV) of the bulk Si-related (Si⁺⁰) component of the Si2p at about 99.5eV. Also the intermediate oxidation components (Si⁺¹, Si⁺², and Si⁺³) can be observed at binding energies between 100 and 103 eV, while the emission from the SiO₂ results in a strong contribution at about 103.5 eV. The photon energy is selected to ensure the highest surface sensitivity as here the photoelectrons come out from the first one to two layers. By comparing the intensities of the oxide and substrate components, it was possible to estimate the SiO₂ thickness to about 0.5 nm for the HfCl₄ and

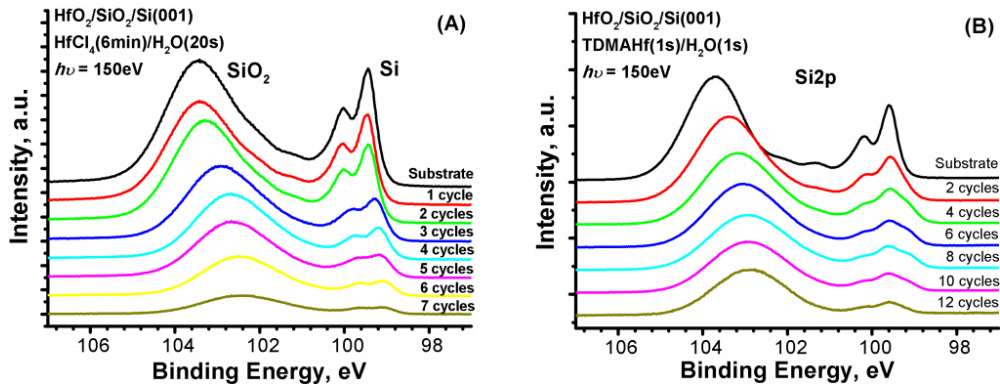


Figure 4.5: Si2p spectra for HfCl₄ (a) and TDMAHf (b). Black lines are the clean substrate, color lines are after complete ALD cycle. The spectra were measured with photon energy of 150 eV. The peaks at about 99.5 eV are due to bulk Si component, and the peaks at about 103.5 eV are due to the SiO₂ component from the substrate. The features between 100 and 103 eV are due to the suboxide components.

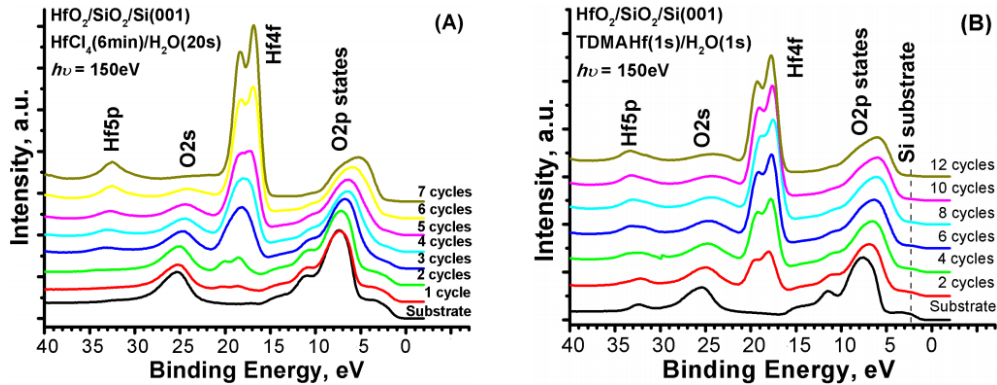


Figure 4.6: VB spectra for HfCl₄ (a) and TDMAHf (b). Black lines are the clean substrate, color lines are after complete ALD cycle. The spectra were measured with photon energy of 150 eV. The major features of the VB and the core level lines are indicated.

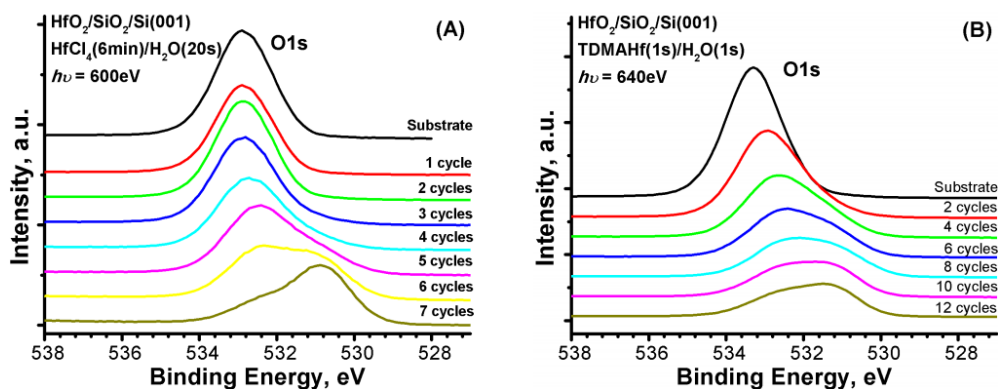


Figure 4.7: O1s spectra for HfCl₄ (a) and TDMAHf (b). Black lines are the clean substrate, color lines are after complete ALD cycle. The spectra were measured with photon energy of 600 eV and 640 eV for HfCl₄ and TDMAHf respectively.

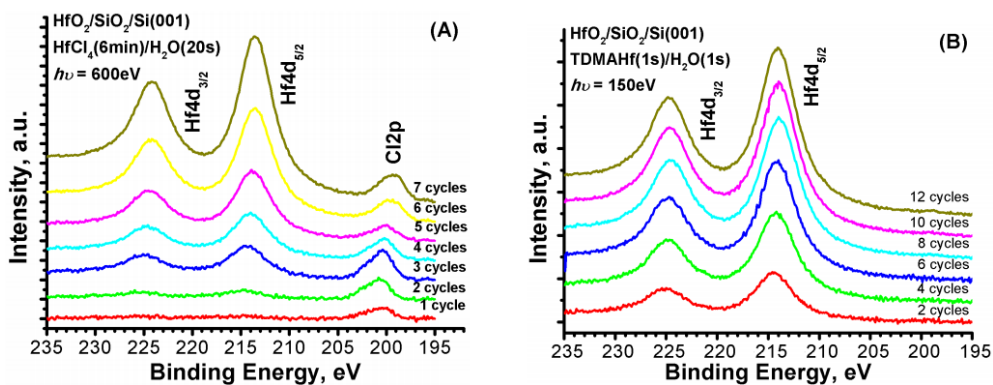


Figure 4.8: Hf4d spectra for HfCl₄ (a) and TDMAHf (b). The background, due to the Si2s plasmon tail from the substrate, was subtracted. The spectra were measured with photon energy of 600 eV and 640 eV for HfCl₄ and TDMAHf respectively.

TDMAHf experiment. Also in the VB regime, we use the high surface sensitivity of the 150 eV excitation energy (Fig. 4.6). Here the substrate emission shows the typical features of the SiO₂ VB [58]. The deposition of HfO₂ results in a shift of the VB maximum from its value of about 5 eV in SiO₂ to a value of about 3 eV in HfO₂. Most prominent are the strong features of the Hf4f levels occurring between 15 and 20 eV. In Fig. 4.7, the O1s spectra measured with photons of 600 eV and 640eV for the HfCl₄ and TDMAHf experiments respectively, are reported. Also in this case, the photon energy is selected for obtaining data with a high surface sensitivity. It should be noted that the gain in sensitivity is about one order of magnitude when comparing to conventional laboratory sources. The variations in the O1s level after each cycle in experiment with the HfCl₄ and TDMAHf precursors, Fig. 4.7(a) and 4.7(b) show first a decrease of the intensity, followed by a shift from 533 to about 532 eV. An emission arises around 530.5 eV that is characteristic for HfO₂ [59] after the 3rd and 8th for the HfCl₄ and TDMAHf experiments respectively. These data clearly show the growth of HfO₂. In Fig. 4.8, we show the photoemission data taken around the Hf4d emission. In all experiment, the emission from the Hf4d levels increase in intensity showing growth of HfO₂. For HfCl₄ data (Fig. 4.8(a)), we find a contribution at around 200 eV, attributed to the Cl2p emission. We have extracted the information about the composition of the overlayer for each cycle by comparing the ratios O/Hf estimated from the intensities of the O1s and Hf4d peaks. Also we should analyze Si2p spectra to determine thickness of overlayer and interfacial layer formation. For obtaining the intensity values, we have executed a fit to the O1s and Si2p spectra in order to separate the SiO₂ component from the HfO₂ in the O1s spectrum and the Si substrate from the Si2p. The fit of Si2p spectra are showed in Fig. 4.9. Before fitting spin orbital splitting was removed using 0.61eV as splitting energy and 0.5 as statistical ratio. The fit was performed using a Levenberg-Marquardt least-square algorithm using Voigt functions. In the fit Si contributions with oxidation states from +0 to the +4 are represented. The shifts peaks relative to the Si⁺⁰ component of Si⁺¹, Si⁺², Si⁺³ and Si⁺⁴ are 0.98eV, 1.85eV, 2.64eV and 3.87eV respectively. For successful fitting we have add two more components Si α and Si β near the bulk peak, at -0.28eV and 0.31eV respectively. Those contributions are addressed to Si-Si bonds in the interface between Si and SiO₂ [60]. The O1s spectra fit is included three components (Fig. 4.10): two strong contributions from SiO₂ and HfO₂ at binding energy 533 and 530.5eV respectively, and small peak at higher binding energy due to CO contaminations. To obtain the intensities of Hf4d peaks area under the curves were taken. The characterization of the Hf-oxide by means of photoemission is usually made considering the energy position of the Hf4f and O1s peaks. We compare the binding energy of our in-situ samples with that present in literature and with other samples produced with standard ALD reactors and measured ex-situ. We find the binding energy of the HfO₂ component in the O1s and Hf4f spectra to be about 530.5 and 17 eV, respectively. Those measured

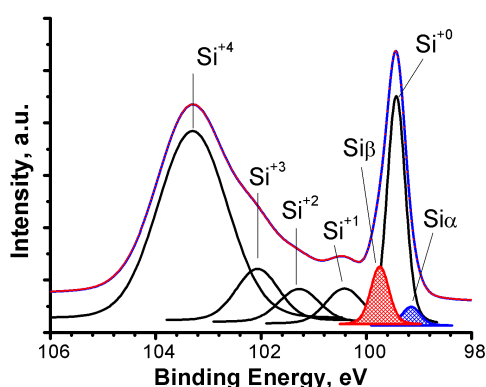


Figure 4.9: The fit Si2p spectra of etched Si/SiO₂ substrate using a Levenberg-Marquardt least-square algorithm using Voigt functions.

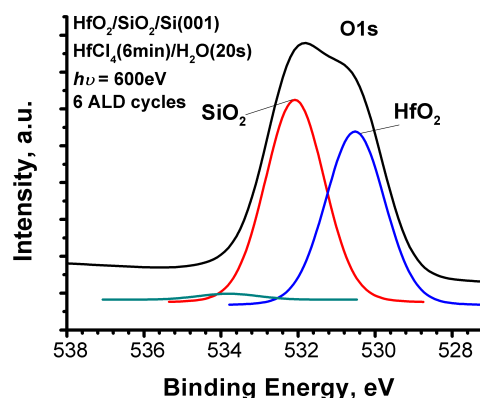


Figure 4.10: The fit O1s spectra after 6 ALD cycle with HfCl₄ precursor

binding energies are very similar to the samples produced in a standard way with no silicate formation, as it would result in a larger binding energy of O1s and Hf4f. We have to note that from the line shape of the Si2p peak it is not easy to determine the presence of silicate because of the existence of suboxide in the same energy range observable in our measurements thanks to the high sensitivity of our setup.

4.2.2 Evolution of interfaces HfO₂/SiO₂/Si

The attenuation of the Si2p peak, due to the elastic and inelastic scattering processes experienced by the electrons of the substrate as they travel through a film of thickness d , will be used to investigate the overlayer thickness as a function of ALD cycle. Also data from Si2p spectra give information about evolution of interfacial layer IL of SiO₂ during ALD growth of HfO₂. From the spectra in Fig. 4.5, we have obtained the intensity values (peak area) of the substrate, oxide and suboxide components of the Si2p level. The ratio between Si⁺⁴ and Si⁺⁰ components are collected in Table 4.1 for both HfCl₄ and TDMAHf experiments. The intensity of two components of Si2p spectra versus ALD cycles are showed in Fig. 4.11 and 4.12 for HfCl₄ and TDMAHf respectively. All lines are normalized to intensity in the etched substrate for a better comparison. The intensity axes are showed in exponential scale. We can note the different attenuation of the bulk Si component at about 99.5 eV and of the SiO₂ component at about 103.5 eV. This fact could be due to the formation of an extra Si-oxide growing at the interface between the substrate and the HfO₂ oxide, as proposed by other authors on the basis of both [33, 61] experimental and theoretical investigations. Actually if we consider ratio between Si⁺⁴ and Si⁺⁰ components and use the equation 2.5, we can calculate growth of IL during ALD. Total thickness and relative growth of IL are reported in Tab. 4.1. For experiment with the HfCl₄

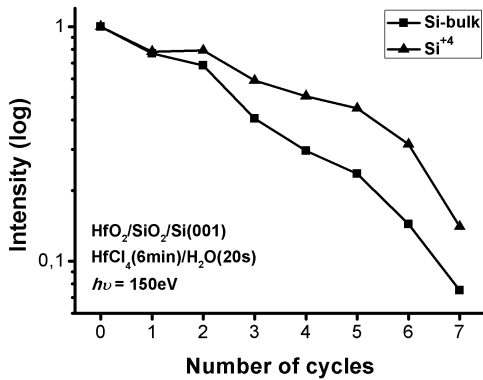


Figure 4.11: Si₂p intensity of the bulk Si and Si⁺ components as function of the ALD cycle using HfCl₄ precursor. The intensity values are reported on a logarithmic scale.

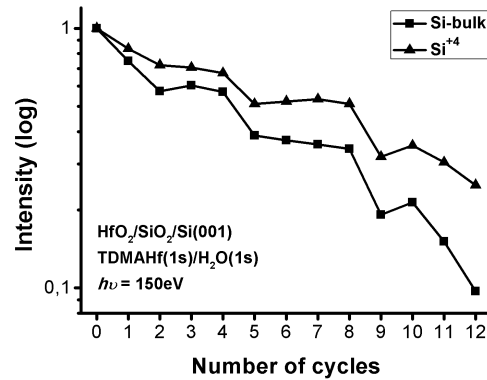


Figure 4.12: Si₂p intensity of the bulk Si and Si⁺ components as function of the ALD cycle using TDMAHf precursor. The intensity values are reported on a logarithmic scale.

precursor initial thickness of Si-oxide layer is 0.47nm what corresponds to about 1 monolayer. The IL growth is about 0.10nm and 0.21nm after three and six ALD cycles. How we will show later 3 and 6 ALD cycle are corresponded to 1ML and 2ML of HfO₂ respectively. It means growth rate of IL is about 0.11nm per 1ML of Hf-oxide. We should note there is no further IL growth after 2 ML of HfO₂. In TDMAHf experiment initial thickness of Si-oxide layer is 0.55nm it is a little bit thicker than for substrate in HfCl₄ experiment. And we have mention that we use silicon substrate with chemical oxide and native oxide in experiments with HfCl₄ and TDMAHf respectively. Estimated growth of IL is 0.11 nm and 0.28 nm after 8 and 12 ALD cycles. From the later analyses we can note that after 8 and 12 ALD cycles thickness of Hf-oxide are about 0.5 and 1.0 nm, 1ML and 2ML respectively. The growth of IL after 1ML HfO₂ is comparison with first experiment, but after second layer of Hf-oxide it is larger and equals 0.17nm. The addition growth of IL can be explained by further analyze of physical properties of Hf-oxide layer. A stoichiometry of this layer shows oxygen-rich Hf-oxide and oxygen can penetrate to substrate and form addition SiO₂. Information about IL growth is important not for only final properties of semiconductor devises, but also for determination properties and growth model of Hf-oxide layer.

4.2.3 Model of growth

We will continue to use the attenuation of the Si₂p peak to investigate the overlayer thickness as a function of ALD cycle and to determine model of HfO₂ growth. Our studying we base on equation $I = I_0 \exp(-\frac{d}{\lambda \cos \theta})$, but we have note, this equations include attenuation from growth Hf-oxide layer and increasing thickness of IL

<i>HfCl₄</i>				<i>TDMAHf</i>			
	Si ⁺⁴ /Si ⁺⁰	<i>t_{IL}</i>	<i>G_{IL}</i>		Si ⁺⁴ /Si ⁺⁰	<i>t_{IL}</i>	<i>G_{IL}</i>
Substrate	2,17	0,47	0,00	Substrate	2,88	0,55	0,00
1 cycle	2,21	0,47	0,01	2 cycles	3,63	0,62	0,07
2 cycles	2,51	0,51	0,04	4 cycles	3,40	0,60	0,05
3 cycles	3,15	0,57	0,10	6 cycles	4,06	0,65	0,10
4 cycles	3,71	0,62	0,15	8 cycles	4,29	0,67	0,12
5 cycles	4,12	0,65	0,18	10 cycles	4,77	0,70	0,15
6 cycles	4,74	0,68	0,21	12 cycles	7,38	0,84	0,29

Table 4.1: Calculated ratio between Si⁺⁴ and Si⁺⁰ components of Si2p spectra, total thickness of interfacial layer *t_{IL}* and IL growth *G_{IL}* during ALD for the etched substrate and after the each ALD cycle for the HfCl₄ and after each two cycles for the TDMAHf.

described above. In this case we should modify this equation:

$$I = I_0 \exp\left(-\frac{d_{HfO_2}}{\lambda_{HfO_2} \cos \theta}\right) \exp\left(-\frac{G_{IL}}{\lambda_{IL} \cos \theta}\right) \quad (4.2)$$

where d_{HfO_2} is the thickness of Hf-oxide overlayer, G_{IL} is the growth of IL during ALD. We know already IL growth and can subtract attenuation due to this growth from the total substrate signal. These data are shown in Fig. 4.13 and Fig. 4.14 for HfCl₄ and TDMAHf respectively. The close line is experimental data and the dash line is calculated using Eq. 4.2. For the experiment with HfCl₄ we obtain for the cycles 3 and 6 an HfO₂ thickness of about 0.45 and 1 nm, respectively. For TDMAHf experiment we obtain the same thickness of HfO₂ layer after 8 and 12 cycles. These thicknesses are very near to the nominal thicknesses of one and two layers, respectively, while the values of the other cycles do correspond to some fractional coverage. This result demonstrates the ALD growth of Hf oxide with a rate of one layer per three cycles for HfCl₄ experiment. We need 8 and more 4 ALD cycles for growing first and second monolayer respectively in the experiment with TDMAHf precursors. In fact, one has to consider that with an ALD growth rate of $1/r$, every layer is completed only after r cycles and only after r cycles the exponential attenuation with a length of $N \times 0.5$ nm may be observed, where N is the number of completed layers. In the intermediate i^{th} cycle, on the other hand, the expected attenuation cannot be purely exponential, but is rather the sum of the exponential attenuation, with exponential index $\exp(-N \times 0.5 / \lambda \cos \theta)$ multiplied by a coverage fraction i/r , and the remaining uncovered surface for which no attenuation is observed. This is therefore smaller than the purely exponential attenuation. This behavior is observed in Fig. 4.13 for the intermediate cycles 1 and 2 and 4 and 5, where the attenuation of the Si2p intensity is smaller than exponential. The deviation from a purely exponential attenuation of the Si2p intensity can be also due

to the formation of islands, but one should not confound the behavior of the intensity attenuation in an ALD growth with that of Stranski-Krastanov and Volmer-Weber growth modes. In the ALD mode, the complete coverage is reached exactly when the layer is completed, while for the island growth this will occur for an average thickness larger than the single layer height. Here we see that after three cycles, corresponding to one layer, the exponential attenuation is restored, indicating the occurrence of the ALD growth. For TDMAHf experiment the situation is more complex. At first there is not constant growth rate. For first layer we need eight ALD cycles and only four ALD cycles to grow second layer. Also attenuation for intermediate ALD cycles is large than the purely exponential attenuation. These behavior can be explained by large changes of physical properties happened during these ALD cycles. We want evidence that a covering of one Hf-oxide layer does not necessarily mean that the density of the HfO₂ is the nominal density of 9.68 g/cm³. To have an estimate of the oxide density independently from the Si2p attenuation, we compared the values of the O and Hf atoms in the Hf-oxide in the first and second layer, and we found a relative changing of density, as it will be shown below. The variation of density may influence the thickness measurement made by X-ray photoelectron spectroscopy, as the attenuation length λ may depend on the actual density of the scattering material [62, 63]. Anyway, the estimation of λ , which is usually made on the base of complex theoretical models, is not unambiguous, and may depend on the measurement geometry [64]. Moreover, when such theoretical models are adopted for the estimation of λ , one should consider that in the monolayer range that estimation may suffer of large uncertainties, and should be corrected for the possible presence of defects related to nonstoichiometry or contaminations. Finally, from the independent observation of the exponential attenuation of the Si2p peak intensity and the calculation of the relative density increase, we find that the actual value of X does depend only slightly from the density of the HfO₂ (less than a 10% increase for a density increase of a factor 2), at least in the first two layers, in accordance with the estimation made by using the QUASES-IMFP-TPP2M software based on the Tanuma-Powell-Penn theory.

4.2.4 Physical properties in-situ prepared layers of Hf-oxide

We have just mentioned that the Si2p attenuation with the ALD growth of Hf-oxide is not univocally related to the actual nature of the Hf-oxide, like its stoichiometry, its density, and the possible presence of contaminations. To investigate these properties, we have used the intensities of the Hf-oxide component in the O1s and the Hf4d, one has to take into account the intensity attenuation experienced by the core electrons in a similar way as described for the Si2p core level. The area Cl2p peaks from contamination by chlorine was taken into account in HfCl₄. The relation between the measured intensity of a core level and the number of the emitting atoms is given by the Eq. 2.2. The determination of reasonable values for the boundaries in the

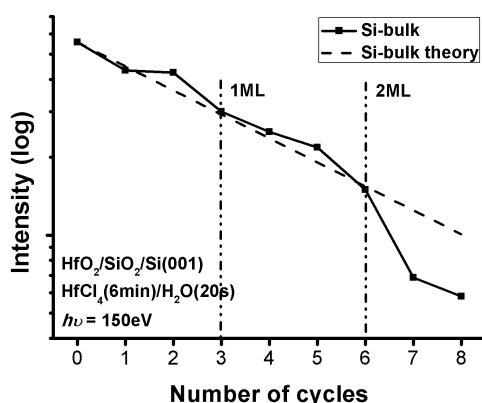


Figure 4.13: The close line is Si2p intensity of the bulk Si component as function of the ALD cycle using HfCl_4 precursor. The dash line is the theoretical exponential attenuation. The intensity values are reported on a logarithmic scale.

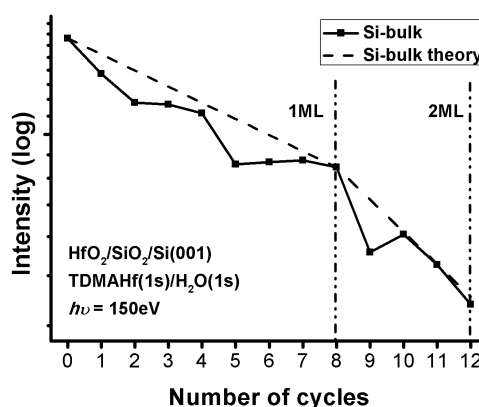


Figure 4.14: The close line is Si2p intensity of the bulk Si component as function of the ALD cycle using TDMAHf precursor. The dash line is the theoretical exponential attenuation. The intensity values are reported on a logarithmic scale.

integrals of that equation may be very difficult when considering amorphous materials. Although the HfO_2 films grown at 300°C are certainly amorphous, it is reasonable to think that in the first layer the O (or Cl) atoms are placed above the Hf atoms and are very near to the vacuum side, while the Hf atoms are near the center of the film, between the vacuum and the interface. This consideration enables us to choose 0.25 nm as x_2 and 0 nm as x_1 for the calculation of the number of O and Cl atoms in the first layer, while for the calculation of the Hf atoms we may reasonably choose $x_1 = 0.25\text{ nm}$ and $x_2 = 0.5\text{ nm}$. For the second layer, where the amorphous nature of the HfO_2 becomes more important, this assumption is not correct anymore (see Fig. 4.17). In this case, we have considered a homogeneous distribution of O, Cl, and Hf atoms in the second layer maintaining the same ordered distribution of atoms in the first layer. By doing this, we have obtained the O/Hf, Cl/Hf, and O + Cl/Hf ratios reported in Fig. 4.15 for the experiment with the HfCl_4 precursor and the O/Hf ratio for the experiment with the TDMAHf precursor. Also data are collected in Table 4.2. If we address to the HfCl_4 experiment, the values of Cl/Hf are very large in the first two cycles, but already in the third cycle that ratio appreciably decreases following an exponential attenuation, leading to the conclusion that Cl contamination is mostly localized at the $\text{SiO}_2/\text{HfO}_2$ interface. On the contrary, the values of the O/Hf atomic ratio are zero in the first two cycles, because of the absence of oxygen atoms bond hafnium, and increase after the third cycle. Except for the first two cycles, the total ratio is almost constant up to the seventh cycle. We want to point out that those values depend on the actual atomic distribution of the Hf, Cl, and O species. In fact,

$HfCl_4$				$TDMAHf$			
	O/Hf	Cl/Hf	Cl+O/Hf		Hf	O_{Hf}	O/Hf
1 cycle	0	1,9	1,9	2 cycles	383778	532625	2,3
2 cycles	0	1,1	1,1	4 cycles	817748	983239	2,7
3 cycles	1,6	0,4	2	6 cycles	844812	1316850	2,1
4 cycles	1,6	0,2	2	8 cycles	892040	1550120	1,9
5 cycles	1,8	0,1	1,9	10 cycles	814995	1704850	2,3
6 cycles	1,9	0,1	2	12 cycles	798918	1848910	2,2

Table 4.2: Calculated ratio between intensity of Hf4d core level and HfO₂ component of the O1s core after the each ALD cycle for the HfCl₄ and after the each two cycles for the TDMAHf.

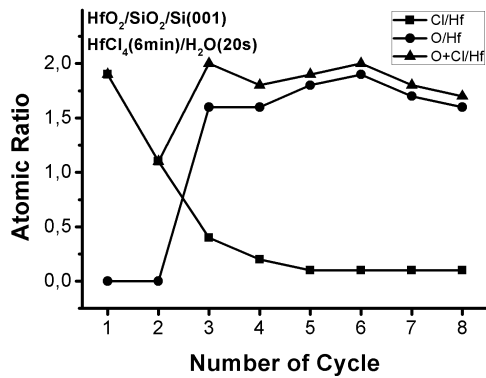


Figure 4.15: O/Hf, Cl/Hf and (O+Cl)/Hf atomic ratios calculated from the intensities (peak area) of the O1s, Hf4d and Cl2p core level lines in HfCl₄ experiment

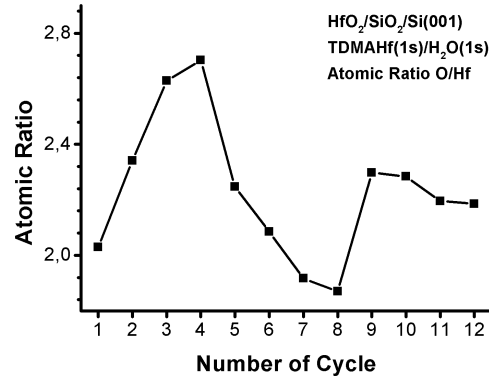


Figure 4.16: O/Hf atomic ratio calculated from the intensities (peak area) of the O1s and Hf4d in TDMAHf experiment

if we consider a completely amorphous Hf-oxide for both the first and second layer, the ratio estimation would be about 20% larger, while for both layers completely ordered the ratio would be about 20% smaller. Within a defined structure model, the error sources are given by the uncertainties on the actual values of σ and λ . These may be estimated to be of the order of 5

On the basis of our experimental results, we can conclude that the film changes its chemical nature while growing during the first cycles. In the first two cycles, the Hf atoms are bond to the substrate oxygen atoms and to the Cl atoms of the HfCl₄ molecule. Between the third and the fifth cycles, the incorporation of O becomes more efficient but it does not reach the saturation, and therefore not all O atoms are bridge bond to the Hf centers. Finally, the building of O bridging bonds takes place, with the increase of the O/Hf ratio and the formation of bulk-like HfO₂ after

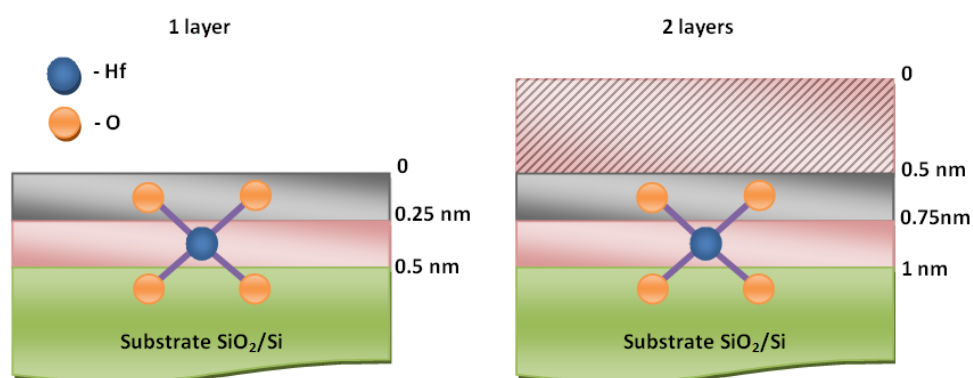


Figure 4.17: Growth model used for calculating the O/Hf ratio in the first and second layer.

the sixth cycle.

These findings compare very well with the results of the XAS measurements at the O1s edge. The line shape of the XAS spectra change abruptly with the sixth cycle, as can be observed in Fig. 4.18. In order to put in evidence this abrupt change, we have calculated the integral of the XAS spectra at the O1s edge for each cycle. The integral of the XAS spectra is related to the number of the emitting atoms and to their chemical state (through the absorption coefficient). When a chemical property, such as bond type or valence state, of the emitting atoms changes, the absorption coefficient also varies, inducing a strong modification of the XAS line shape and of the integral intensity. Also the variation of the number of emitting atoms leads to modifications in the integral of the XAS signal, but these are usually very small and are not accompanied by mutations of the line shape. In Fig. 4.19, we report the measured values of the integral intensity as well as the signal-to-background (S/B) ratio as a function of number of cycle. The S/B ratio is proportional to the number of O atoms involved in the x-ray absorption and has an almost linear behavior with increasing HfO₂ thickness. On the contrary, the increase of the integral value is initially linear, up to the cycle number 5, changing its behavior from the cycle number 6. The abrupt variation of slope observed with the sixth cycle in the integral intensity is not observed in the S/B ratio indicating a mutation in the chemical property of the HfO₂. The line shapes of the XAS spectra for the cycles six to eight are different from the previous ones and are very similar to those of bulk HfO₂ reported in literature, presenting the two characteristic sharp peaks at 533 and 537.5 eV. With the sixth cycle, the second layer is completed, and therefore the contribution of the SiO₂ from the substrate becomes very weak. The difference in the integral of the XAS spectra is related to the mutation between the first layer, where the HfO₂ is very sparse, and the second layer, for which the HfO₂ is dense and bulk like. In fact, in the first layer, the Hf atom is bond to the O atoms from the substrate (bond to Si), to

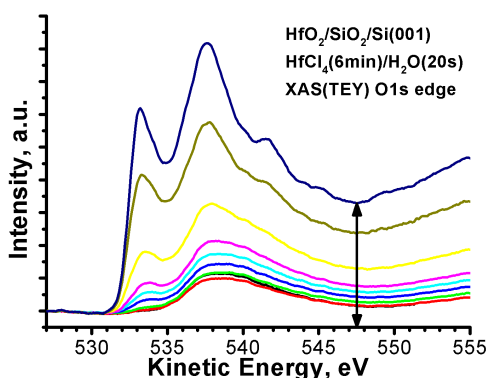


Figure 4.18: TEY spectra at the O1s edge of clean substrate (black line) and after each ALD cycle with HfCl_4 precursor up to the eight (dark blue line). The raw spectra were divided by the incoming photon flux and then linear background was subtracted.

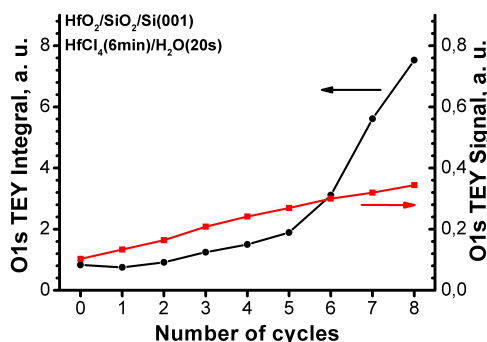


Figure 4.19: Integral intensity (red line) and S/B ratio (black line) values of the O1s TEY for the clean substrate and after each ALD deposition cycle. The increase of the TEY integral intensity is almost linear up to the fifth cycle and then changes at the sixth cycle. Between sixth and eighth cycles, the increase is again linear but steeper.

Cl atoms (as was shown above), and to the OH groups, and it cannot be defined as bulk-like because the bridging O are very rare and both the oxygen and hafnium atoms are undercoordinated. On the contrary, the second layer is denser than the first one and with an almost ideal stoichiometry, meaning that the bridging O atoms are much more abundant and with the correct coordination. The Hf atoms are bonded to the O from the HfO_2 of the first layer and the OH groups on the surface in an almost bulk-like configuration. In the experiment with TDMAHf precursor behavior of O/Hf is different. We should note that contamination from TDMAHf ligands contains nitrogen and carbon atom and can not be distinguished from substrate contamination. But level of this contamination is very small and can be neglected. Using model of growth of Hf-oxide described above, we calculated the ratio O/Hf. These values are plotted in Fig. 4.16. Already after first cycle stoichiometry of Hf-oxide is two. In the next three cycles the ratio grows up to 2.7 value. It means after the fourth ALD cycle we have oxygen rich Hf-oxide. Actually if we compare VB band spectra of the TDMAHf and HfCl_4 experiments Fig. 4.6, we can note relatively large intensity of the O2s and O2p states in comparison with the Hf4f levels in the TDMAHf experiments. Then the next 4 cycles up to the eighth ALD cycle the ratio goes down and equals 1.8 after the eighth ALD cycle (1 layer). The start of the growth of the second layer is accompanied by the O/Hf ratio growth. The stoichiometry after the ninth ALD cycle is 2.3. The subsequent ALD growth shows decreasing of the

O/Hf ratio. And after completed second layer it equals 2.2. Excess oxygen atoms in the Hf-oxide layer is defects. They work like additional scattering points. And this information gives possibility to explain larger attenuation of the substrate signal Fig. 4.14 after intermediate cycles 2-7 and 9-11.

4.2.5 Contamination content in the HfCl_4 experiment

The variation intensity of O1s and Cl2p during ALD can give important information. In relation to these experimental results the origin of the Cl contamination proposing a mechanism based on the adsorption geometry of HfCl_4 onto the -OH terminated substrate. Those variations could not be observed in the ex-situ experiments as the films were investigated after a certain number of cycles, and the information obtained there was an averaged one. We find that the oxidation step in the first two cycles is very ineffective as no HfO_2 component in the O1s was observed [see Fig. 4.21]. On the contrary, the Cl2p intensity increases constantly in the first three cycles [Fig. 4.20]. The low efficiency in the first oxidation steps leads to the Cl contamination of the HfO_2 at the $\text{SiO}_2/\text{HfO}_2$ interface. At the third cycle, when the effectiveness of the oxidation increases steeply and water reacts with the adsorbed molecule, the Cl content still increases linearly with a slope of 275 a.u. The amount of Hf and O deposited at the third cycle is much larger than in the previous two cycles. This fact reduces the Cl contamination of the first Hf-oxide layer to 20%. In the fourth and fifth cycles the amount of Cl decreases: this could occur if the chlorine atoms were covered by stoichiometric HfO_2 . If we suppose that all Cl atoms were covered after the fifth cycle, then that attenuation should be of the form: $I = I_0 \exp(-d/\lambda \cos \theta)$, with $d = 0.5$ nm, $\lambda = 1.2$ nm, and $\theta = 45$. Anyway, the value measured after the fifth cycle is smaller than the expected one. This leads to two possible scenarios: (1) the Cl atoms were not only covered by new HfO_2 but also removed (at least 20% of the initial quantity), most probably during the oxidation steps of cycles 4 and 5; (2) those Cl atoms were not covered at all and the decrease of Cl intensity is only due to the reaction of the Cl atoms of the first layer with water during the fourth and fifth cycles. In this case only 45% of the Cl incorporated in the first layer withstands the oxidation.

At the sixth cycle the Cl2p intensity again increases. The increase with respect to the fifth cycle is 227 a.u., i.e., similar (although smaller) to the constant value observed in the first layer. This result indicates that when new Cl is introduced into the film it is always done with the same quantity. We turn now to a discussion on the possible reactions taking place at the surface when HfCl_4 is introduced into the system. The HfCl_4 molecule may interact with the-OH terminated surface by ligand exchange with either one, or two -OH groups [32], leading to two different adsorption geometries: an apical attachment, resulting in the adsorbed species -O- HfCl_3 and the release of one Cl atom through the formation of one HCl molecule; or an edge attachment, resulting in the adsorbed species -O- HfCl_2 and the release of

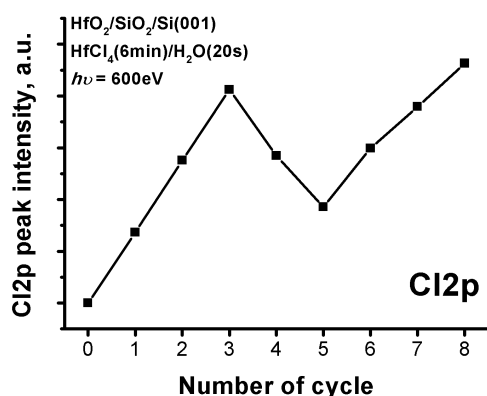


Figure 4.20: Peak the of the Cl2p for each ALD cycle for the HfCl₄ experiment.

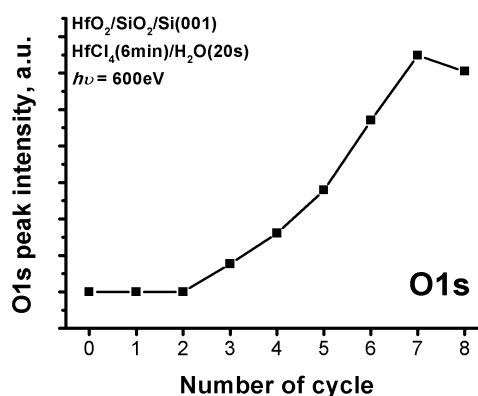


Figure 4.21: Intensity of O1s core levels of Hf-oxide component for each ALD cycle for the HfCl₄ experiment.

two Cl atoms through the formation of two HCl molecules. Another possible reaction is that of HfCl₄ dissociated in oxygen bridges on silica, proposed for the ALD of TiO₂ by Hair and Hertl, and Kynney and Staley, but its occurrence is still a matter of debate. The ligand-exchange reactions are discussed in various theoretical works that address the observed GPC in the ALD of HfO₂ with HfCl₄ and H₂O to the steric hindrance of the adsorbed species or the hydroxylation of the substrate [32]. Ylilammi [29] showed that the observed GPC is in agreement with the occurrence of the edge attachment only, while Green and Alam calculated that the adsorption complexes should be 39% of type-HfCl₃ and 61% of type-HfCl₂ for explaining the observed GPC by means of steric hindrance alone [30]. The energy balances of the two geometries are different because the apical geometry, with only one ligand exchange, needs a smaller activation energy than the edge geometry. Moreover, the probability of adsorption for the two geometries depends also on the density of -OH groups at the substrate, as for the edge geometry [30] two-OH groups are needed, while for the apical geometry [30] only one -OH group is necessary, see Fig. 4.22. Unfortunately, at present there is no theoretical investigation dedicated to compare the energy balancing of the two adsorption geometries in order to predict the occurrence of one or the other geometry. Actually, it is possible that the probability for the two geometries depends on the substrate. This was not explicitly considered in the theoretical investigations present in literature, with the exception of the work of Puurunen [32] and Deminsky et al. [65], where the authors consider the surface hydroxylation or dehydroxylation to simulate the experimentally observed GPC or their dependence on the temperature. Deminsky et al. proposed a mechanism for the inclusion of Cl into the oxide film based on the steric repulsion between chemisorbed surface groups and adsorbed HfCl₄ molecules [65]. We interpret the observation that chlorine is incorporated always at fixed quantity as a consequence of the adsorption geometry. The HfCl₄ adsorbed in

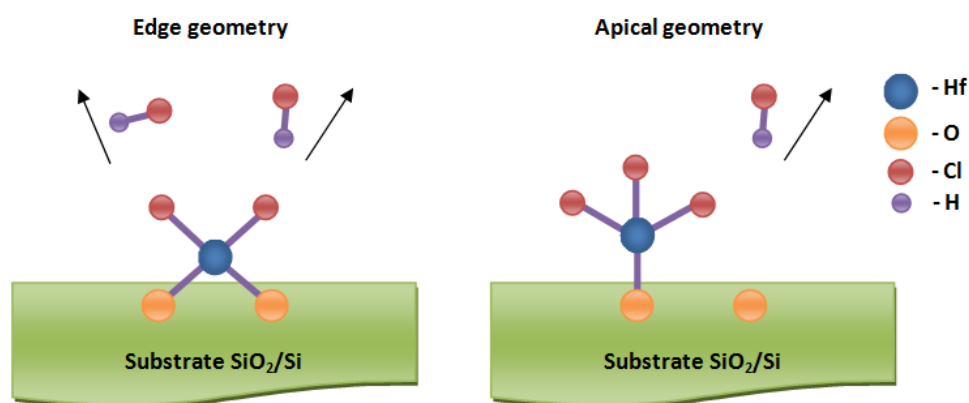


Figure 4.22: Representation of the two ligand-exchange geometries.

a definite geometry does not react efficiently with H_2O to exchange the Cl atoms with the $-\text{OH}$ group, as that reaction is hindered. That geometry can be called for the moment hindering geometry. The other geometry can be called catalyzing geometry, as the molecules adsorbed in that geometry oxidize very efficiently. In the first two cycles only the hindering geometry is observed and produces a Cl-rich chemical adsorbate, while in the third cycle both geometries are possible and the observed ratio between the hindering and the catalyzing geometries is about 9:100. That ratio is calculated considering the ratio between the Cl and the Hf increases in the third cycle. Those increments were then normalized assuming that every HfCl_4 adsorbed in the hindering geometry introduces two Cl atoms in the film, as observed after the first cycle. So, we consider as hindering the edge geometry, with a Hf atom bond to two O from the substrate and two Cl atoms. The hindering geometry could be preferred in the first two cycles because of defects and/or atomic roughness on the substrate surface. If one considers the dissociative adsorption of water that could occur during the oxidation steps, where O atoms from the substrate react with H_2O forming two $-\text{OH}$ groups on the substrate surface, one could suppose that the two groups would participate to the ligand-exchange reaction with the edge geometry. The surface defects and/or atomic roughness could capture the $-\text{OH}$ groups allowing only $-\text{OH}$ couples and enabling only the edge geometry. During the first two cycles the adsorption of HfCl_4 occurs only at those sites; in the third cycle the remaining surface is completely covered and the observed ratio between the two geometries would be the statistical ratio. The Cl atoms resulting from the HfCl_4 adsorbed in edge geometry are oxidized with more difficulty, having a higher activation energy compared to those in the apical geometry, possibly because of the dependence of the activation energy for the oxidation reaction on the interaction of the Cl atoms among them and with the neighboring metal atoms. During the formation of the second layer, the adsorption of HfCl_4 is not possible on those sites terminating with the Cl atoms as no ligand exchange is possible, but the oxidation steps in the fourth

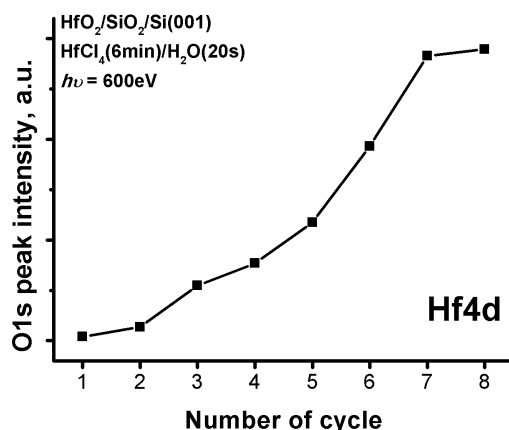


Figure 4.23: Intensity of Hf4d core levels of Hf-oxide component for each ALD cycle for the HfCl_4 experiment.

and fifth cycles may remove a part of the Cl atoms still present in the first layer. Finally, in the sixth cycle the statistical ratio is again obtained, and the increase in Cl2p intensity is once more observed. This mechanism would be in agreement with the nonlinear increase in the Hf4d intensity (See Fig. 4.23), that is very strong at the third and sixth cycles. At those cycles both adsorption geometries are possible and the total adsorption probability is increased with respect to the first and second, and to the fourth and fifth cycles where one geometry is preferred to the other. Finally, it is worth to note that, as already observed from other authors, the presence of Cl atoms as substitutional impurity produces at least one cation vacancy in its nearest neighborhood because of the larger ionic radius of Cl compared to that of O [65]. The Hf vacancy could then bring stress into the oxide film that could be relaxed by releasing the Cl atom, substituting it with O. The stress relaxation would then give the energy necessary for the additional oxidation of the first layer during the growth of the second layer.

4.3 In-situ study of individual steps of ALD process

An important advantage of the in-situ approach in ALD experiments is possibility to measure a sample after each individual ALD steps: after metallic precursor pulse and oxidation. In this experiment we can exactly observe the absorption geometry of precursor, the efficiency of the oxidation step and follow IL changing during ALD process. We carried out the experiment with TEMAHf like metallic precursor and water, in which we made 3 complete ALD cycles and measured the sample after precursor and oxidation pulses. The XPS spectra of O1s, VB, Si2p and C1s are

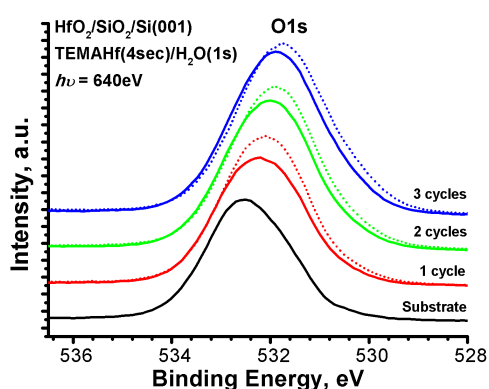


Figure 4.24: Spectra of O1s core levels for substrate (black line), after the precursor and oxidation pulses (close and dot color line, respectively) for TEMAHf experiment.

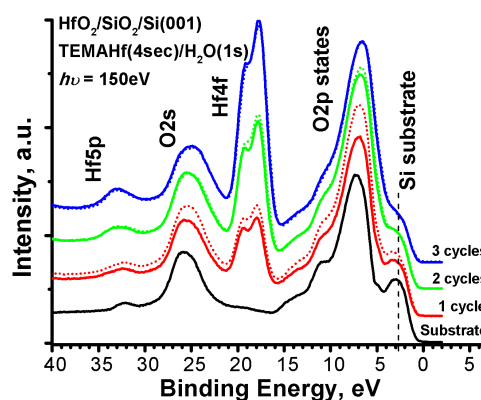


Figure 4.25: Spectra of VB core levels for substrate (black line), after the precursor and oxidation pulses (close and dot color line, respectively) for TEMAHf experiment.

showed in Fig. 4.24, Fig. 4.25, Fig. 4.26 and Fig. 4.27 respectively. At first we measure clean substrate after HF etching (black line). Then we make the usual metallic precursor pulse with following nitrogen purge and measure the sample (color close curves). After these measurements oxidation is made with following nitrogen purge (color dot curves). In that way we complete the first ALD cycle and in the similar way investigate the next cycles. Unfortunately this experiment was not so good. Experimental parameters were wrong. At first the substrate temperature was too high, more than 350°C. And silicon dioxide was too thin with island surface. These reasons resulted in complex growth (not ALD) Hf-oxide and silicate formation in the interface. It leads to not possibility to make quantitative analysis. Nevertheless even this experiment show large advantageous in comparing with ex-situ experiment. Here we can follow spectra shape changing after precursor and oxidation steps. In Fig. 4.24 you can see O1s spectra. After the first metallic precursor pulse there are large changes in comparison with substrate spectra. The peak becomes broader due to second component of Hf-O bonds at lower binding energy. Hafnium content onto the sample is confirmed by VB spectrum in Fig. 4.25. We can observe the Hf4f peak at about 18eV. Also large changes happen after the oxidation pulse. The total intensity of O1s increases because of growth of IL and particularly a replacing of TEMA ligands by OH groups. The replacing of TEMA ligands is evidence in the shape changing Hf4f peak in VB spectra, and in the growth of oxygen 2s and 2p states. The next XPS spectra show similar behavior. After the metallic precursor we have shift in O1s spectra and increasing intensity of the Hf4f peak. The following oxidation lead to further shift of O1s together with growth of total intensity. The changing of Hf4f can be observed, but it is smaller in comparison with the first cycle.

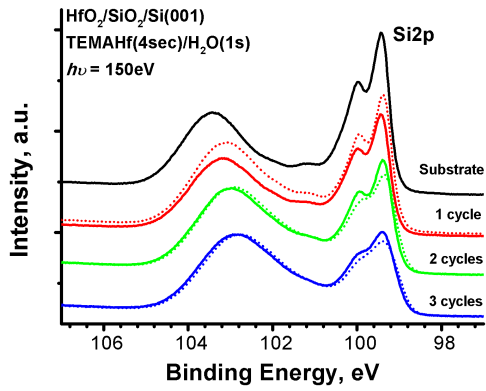


Figure 4.26: Spectra of Si2p core levels for substrate (black line), after the precursor and oxidation pulses (close and dot color line, respectively) for TEMAHf experiment.

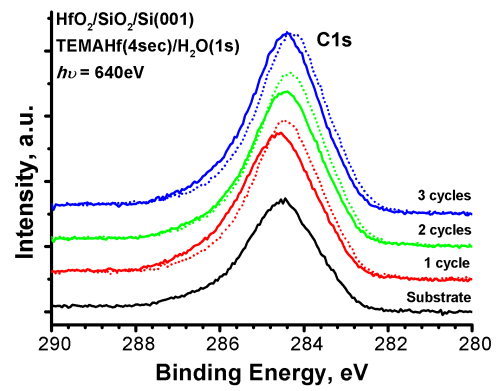


Figure 4.27: Spectra of C1s core levels for substrate (black line), after the precursor and oxidation pulses (close and dot color line, respectively) for TEMAHf experiment.

The evolution can be observed also in Si2p and C1s spectra in Fig. 4.26 and C1s respectively. From Si2p spectra is evidence the changing in chemical properties of overlayer what is resulted in different attenuation of the silicon substrate signal.

Chapter 5

Conclusions

We have studied the ALD growth of HfO_2 in the very early stages making use of SR based photoemission and XAS. The quality of the film was comparable to those grown in commercial ALD reactors for both HfCl_4 and TDMAHf precursors. We have observed that the growth proceeds homogeneously also in the monolayer range, without formation of islands. The growth rate for HfCl_4 precursor we have obtained is one layer per three cycles and is not linear within the layer completion. During the third and sixth cycles, the growth accelerates to complete the first and second layer, respectively. We have also observed that the first layer is very sparse, while the second one has probably the nominal density of HfO_2 . The first layer has a large density of Cl contamination that remains localized most probably at that interface, as also observed by Ferrari et al [66]. These observations were possible thanks to the high resolution photoemission and XAS measurements that were made in situ, avoiding any contamination of the layers and allowing the study of fractional covered surfaces. A very important further remark that we can make is that during the first two cycles, the oxidation step was not successful and started becoming effective only within the third cycle with the completion of the first layer. This observation is in good accordance with the findings of Frank et al. They have observed that the initial growth of Al_2O_3 on H/Si with trimethyl aluminum (TMA) and D_2O proceeds through a nucleation step where the Al on the surface, delivered with the TMA, acts as a catalyst for the oxidation step and the formation of Al_2O_3 . In addition to the results of Frank et al. [34], we observe that after the first two nucleation cycles, the HfO_2 growth changes abruptly in the third cycle with the completion of a very sparse first layer, which cannot be densified with a further cycle as the second layer starts to grow already with the fourth cycle. The growth of the second layer is also accompanied by an abrupt change occurring at the sixth cycle as observed in the XAS spectra. In that case, the transition from nonstoichiometric Hf-oxide to stoichiometric bulk-like HfO_2 can be deduced by the modification of the XAS line shape, confirming the findings

we obtained with photoemission. Our results shed light on the understanding of the early growth of high-k oxides on Si. In particular, we show that the oxidation steps in the very first cycles are critical for the final properties of the oxide/ semiconductor system, as the Cl contamination at the SiO₂/HfO₂ takes place during those early cycles. The growth rate for TDMAHf is not constant. The first layer is completed after 8 cycles and the second layer after the next four ALD cycles. The properties of obtained layer show oxygen rich Hf-oxide content for the intermediate ALD cycles. We think it lead to larger growth of IL of SiO₂ during ALD in comparison with HfCl₄ precursor.

We have shown the evolution of the Cl2p intensity during the ALD growth of the HfO₂ film, observing a nonmonotonic behavior. Our results permit a new possible interpretation of the adsorption and reaction mechanism leading to the formation of HfO₂: we address those intensity variations to the dependence of the adsorption geometry of the HfCl₄ molecule on the presence of defects and/or atomic roughness at the substrate surface. This interpretation was possible because the in-situ approach delivers detailed information on the properties of the film and the substrate after each single ALD cycle, while the ex situ experiments give only averaged information. Our proposed mechanism may lead to new theoretical investigations as it should be confirmed by the energy balancing of the two main reaction mechanisms, namely, the ligand exchange with one or two -OH groups, which were not yet compared in detail. We conclude that the one-ligand exchange is energetically favored with respect to the two-ligands exchange, and that the oxidation reaction after the two-ligand exchange reaction needs a larger activation energy than the one-ligand exchange. The combination of these two properties leads to the presence of Cl contamination in the HfO₂ films. For removing it, one should increase the efficiency of the oxidation step, for example, by using ozone, although ozone would increase the thickness of the SiO₂, especially during the first two ALD cycles, in which the SiO₂ surface is also exposed to the oxidant. Ozone would further oxidize the initial SiO₂ and the interfacial layer would increase. The increase of SiO₂ is unwanted in the practical use of HfO₂, because a thick SiO₂ would decrease the EOT of the Si/SiO₂/HfO₂ stack. Also we showed that one of the greatest advantages in using our method is the possibility to maintain a very reactive surface (like the surface partially covered with unreacted HfCl₂ and partially terminated with SiO₂) for a relatively long time in the same physical-chemical status, thanks to the UHV conditions. It would be impossible to perform an ex situ experiment on a SiO₂ surface after only one ALD cycle because moisture in the ambient air would react with the substrate and the Cl atoms immediately. We reported that in-situ investigation gives possibility to study individual steps of ALD process and follows reactions occurring after a precursor and oxidation pulses. This type of experiments allows more accurate studying the growth model and the absorption geometry in ALD. We show that the very high sensitivity of photoemission coupled with SR may be a very useful tool for investigating the

properties of ALD films in the sub-monolayer range. And of course we should note that most of all obtained properties can be investigated by in-situ experiments only, and usually ex-situ experiments miss this information.

Bibliography

- [1] M. R. Wordeman G. Bacarani and R. H. Dennard. IEEE Trans. Electron Devices 31, 452, 1984. [cited at p. 1]
- [2] T. Hori. *Gate Dielectrics and MOS ULSIs*. Springer, New York, 1997. [cited at p. 1]
- [3] <http://www.intel.com/technology/silicon/micron.htm>. [cited at p. 2]
- [4] T. Vogelsang and H.R. Hoffman. Appl. Phys. Lett. 62, 2853, 1993. [cited at p. 2]
- [5] M. Fischetti and S. Laux. J. Appl. Phys., 80, 2234, 1996. [cited at p. 2]
- [6] K.K. Chan H.-S. P. Wong and Y. Taur. IEDM Tech. Digest, 427, 1997. [cited at p. 2]
- [7] K. Charles D. Hisamoto L Chang J. Kedzierski E. Anderson H. Takeuchi Y.-K. Choi K. Asano V. Subramanian T.-J. King J. Bokor C. Hu X. Huang, W.-C. Lee. IEDM Tech. Digest, 67, 1999. [cited at p. 2]
- [8] E.J. Nowak T. Kanarsky J.H. Rankin H. Hanafi W. Natzle D. Boyd J. Kedzierski., D.M. Fried. IEDM Tech. Digest, 437, 2001. [cited at p. 2]
- [9] S. Kalpat M. Zavala T. Stephens R. Mora S. Bagchi C. Parker J. Vasek-D. Sing R. Shimer L. Prabhu G.O. Workman G. Ablen Z. Shi J. Saenz B. Min D. Burnett B.-Y. Nguyen J. Mogab M.M. Chowdhury W. Zhang J.G. Fossum L. Mathew, M. Sadd. IEDM Tech. Digest, 713, 2005. [cited at p. 2]
- [10] R. Rios and N. D. Arora. Tech. Dig. Int. Electron Devices Meet., 613, 1994. [cited at p. 3]
- [11] J.D. Plummer and P.B. Griffin. Proc. IEEE 89, 240, 2001. [cited at p. 4]
- [12] J. Robertson. J. Vac. Sci. Technol. B 18, 1785, 2000. [cited at p. 4]
- [13] H.J. Hubbard and D.G. Schlom. J. Mater. Res. 11, 2757, 1996. [cited at p. 4]
- [14] D.G. Schlom and J.H. Haeni. MRS Bull. 127, 98, 2002. [cited at p. 4]
- [15] M. Gribelyuk M. Copel and E. Gusev. Appl.Phys.Lett. 76, 436, 2000. [cited at p. 5]
- [16] C.L. Liu M.Stoker R.I. Hegde R.S. Rai M. Gutowski, J.E. Jaffe and P.J. Tobin. Appl. Phys. Lett 80, 1897, 2002. [cited at p. 5]

- [17] A. Chin W.J. Chen Y.H. Wu, M.Y. Yang and C.M. Kwei. IEEE Electr.Device L. 21, 341, 2000. [cited at p. 5]
- [18] J. Kwo et al. ,Appl. Phys. Lett 77, 130, 2000. [cited at p. 5, 19]
- [19] E. Bugiel A. Fissel, H.J. Osten. J. Vac. Sci. Technol. B 21, 1765, 2003. [cited at p. 5]
- [20] H. Ishiwara S. Ohmi, M. Takeda and H. Iwai. J. Electrochem. Soc. 151, G279, 2004. [cited at p. 5]
- [21] A. Rahtu P.I. Raisanen M. Ritala, K. Kukli and M. Leskela. Science 288, 319, 2000. [cited at p. 6]
- [22] J.Robertson. Eur. Phys. J.: Appl. Phys. 28, 265, 2004. [cited at p. 7]
- [23] R. DeJule. Semiconductor international, Issue 11, 2007. [cited at p. 7]
- [24] T. Ghani M.T. Bohr, R.S. Chau and K. Mistry. IEEE Spectrum 44, 29, 2007. [cited at p. 7]
- [25] V. Narayanan E.P. Gusev and M.M. Frank. IBM J. Res. Dev. 50, 387, 2006. [cited at p. 7]
- [26] A. Kasikov H. Mandar R. Rammula J. Aarik, A. Aidla and V.Sammelseg. Appl. Sur. Science, 252 16, 5723, 2006. [cited at p. 7]
- [27] J.W. Maes P. Bajolet B. Brijs E. Cartier T. Conard S. DeGendt O. Richard-W. Vander- vorst C. Zhao M. Green W. Tsai A. Delabie, M. Caymax and M.M. Heyns. Mater. Res. Soc. Symp. Proc. 745, 179, 2003. [cited at p. 7]
- [28] B. Busch G.D. Wilk T. Sorsch T. Conard B. Brijs M.L. Green, M.-Y. Ho, D.Muller M. Bude W. Vandervorst, P.I. Raisanen, and J. Grazul. J. Appl. Phys. 92, 7168, 2002. [cited at p. 7]
- [29] M. Ylilammi. Thin Solid Films 279, 124, 1996. [cited at p. 7, 36]
- [30] M.A. Alamand and M.L. Green. J. Appl. Phys. 94, 3403, 2003. [cited at p. 7, 36]
- [31] R.L. Puurunenand and W. Vandervost. J. Appl. Phys. 96, 7686, 2004. [cited at p. 7]
- [32] R.L. Puurunen. J. Appl. Phys. 95, 4777, 2004. [cited at p. 7, 35, 36]
- [33] J. Wolstenholme P. Mack, R.G. White and T. Conard. Appl. Surf. Sci. 252, 8270, 2006. [cited at p. 7, 27]
- [34] Y.J. Chabal M.M. Frank and G.D. Wilk. Appl. Phys. Lett. 82, 4758, 2003. [cited at p. 7, 41]
- [35] A. Ghatak-Roy S. Terada B. Bunday H. Yeung A. Diebold P.Y. Hung, C. Gondran. J. Vac. Sci. Technol. B 23,2244, 2005. [cited at p. 7]
- [36] Y.J. Chang T.W. Noh R. Jung D.-Y. Cho, S.-J. Oh and J.-C. Lee. Appl. Phys. Lett. 88, 193502, 2006. [cited at p. 7]
- [37] J. Schmitz M. Sturm A. Zinine H. Wormeester R. Bankras, J. Holleman and B. Poelsema. Chem. Vap. Deposition 12, 275, 2006. [cited at p. 7]
- [38] T. Suntola and J. Antson. US Patent 4 058 430, 1977. [cited at p. 9]

- [39] M. Leskela and M. Ritala. *Angew. Chem. Int. Ed.* 42, 5548, 2003. [cited at p. 9]
- [40] J. Niinisto M. Putkonen L. Niinisto, J. Paivasaari and M. Nieminen. *Phys. Stat. Sol. A* 201, 1443, 2004. [cited at p. 9, 10]
- [41] M. Ritala L. Niinisto and M. Leskela. *Mater. Sci. Eng. B* 41, 23, 1996. [cited at p. 9]
- [42] M. Leskela and M. Ritala. *Thin Solid Films* 409, 138, 2002. [cited at p. 9]
- [43] L. Niinisto. *Curr. Opin. Solid State & Mater. Sci.* 3, 147, 1998. [cited at p. 9]
- [44] R.L. Puurunen. *J. Appl. Phys.* 97, 121301, 2005. [cited at p. 9]
- [45] T. Suntola. *Appl. Surf. Sci.* 100/101, 391, 1996. [cited at p. 10]
- [46] J. Niinisto. Ph.D. Thesis, Helsinki University of Technology, 2006. [cited at p. 17]
- [47] <http://www.ni.com/labview/>. [cited at p. 17]
- [48] <http://www.advantech.com>. [cited at p. 17]
- [49] M. Tiitta. Doctoral (Tech.) thesis, Helsinki University of Technology, Espoo, 1998. [cited at p. 19]
- [50] M. Fleisher and H. Meixner. *Sens. Actuators B* 5, 115, 1991. [cited at p. 19]
- [51] M. Fleisher T. Schwebel and H. Meixner. *Sens. Actuators B* 65, 176, 2000. [cited at p. 19]
- [52] M. Fleischer and H. Meixner. *Sens. Actuators B* 6, 257, 1992. [cited at p. 19]
- [53] H. Meixner F. Reti, M. Fleischer and TITLE = J. Giber. [cited at p. 19]
- [54] R. Rizza G. Spoto E. Ciliberto, R. Fragal and G.C. Allen. *Appl. Phys. Lett.* 67, 1624, 1995. [cited at p. 19]
- [55] M. Fleischer T. Weh and H. Meixner. *Sens. Actuators B* 68, 146, 2000. [cited at p. 19]
- [56] K. Dwight Y.-M. Gao, P. Wu and A. Wold. *J. Solid State Chem.* 90, 228, 1991. [cited at p. 19]
- [57] M. Fleischer and H. Meixner. *Sens. Actuators B* 4, 437, 1991. [cited at p. 20]
- [58] M. Tallarida and D. Schmeisser. *Mater. Sci. Eng., B* 144, 23, 2007. [cited at p. 26]
- [59] M. Cho C.S. Hwang J.-C. Lee, S.-J. Oh and R. Jung. *Appl. Phys. Lett.* 84, 1305, 2004. [cited at p. 26]
- [60] O. Yazyev and A. Pasquarello. *Phys. Rev. Lett.*, 96(15) 157601, 2006. [cited at p. 26]
- [61] C. Tang and R. Ramprasad. *Phys. Rev. B* 75, 241302, 2007. [cited at p. 27]
- [62] P.J. Cumpson and M.P. Seah. *Surf. Interface Anal.* 25, 430, 1997. [cited at p. 30]
- [63] C.J. Powell S. Tanuma and D.R. Penn. *Surf. Interface Anal.* 21, 165, 1994. [cited at p. 30]
- [64] M.P. Seah and S.J. Spencer. *Surf. Interface Anal.* 33, 515, 2003. [cited at p. 30]
- [65] M. Deminsky et al. *Surf.Sci.* 549, 67, 2004. [cited at p. 36, 38]
- [66] C. Wiemer S. Ferrari, G. Scarel and M. Fanciulli. *J. Appl. Phys* 92, 7675, 2002. [cited at p. 41]

List of publications

In-Situ Studies of ALD Growth of Hafnium Oxide Films

K. Karavaev, K. Kolanek, M. Tallarida, D. Schmeisser

Advanced Engineering Materials 11/4 (2009) 264-268

HfO₂/Si interface formation in atomic layer deposition films: an in situ investigation

M. Tallarida, **K. Karavaev**, D. Schmeisser

Journal of Vacuum Science and Technology B 27/1 (2009) 300-304

Optimization of the AlON buffer layer for Pr_xO_y/Si stacks

K. Henkel, Y. Burkov, **K. Karavaev**, M. Torche, C. Schwiertz, D. Schmeisser

Journal of Vacuum Science and Technology B 27/1 (2009) 253-257

The initial atomic layer deposition of HfO₂/Si(001) as followed in situ by synchrotron radiation photoelectron spectroscopy

M. Tallarida, **K. Karavaev**, D. Schmeisser

Journal of Applied Physics 104 (2008) 064116

HfO₂ ALD-growth studied by in situ photoemission

M. Tallarida, **K. Karavaev**, D. Schmeisser, E. Zschech

Proceedings of 15th Workshop on Dielectrics in Microelectronics (2008) 289-290

Al-Oxynitride as a buffer layer for high-k dielectrics

K. Henkel, Y. Burkov, M. Bergholz, **K. Karavaev**, R. Sohal, M. Torche, D. Schmeisser

Proceedings of 15th Workshop on Dielectrics in Microelectronics (2008) 161-162

Al-Oxyxynitride interfacial layer investigations for Pr_xO_y on SiC and Si

K. Henkel, **K. Karavaev**, M. Torche, C. Schwiertz, Y. Burkov, D. Schmeisser
Journal of Physics: Conference Series 94 (2008) 012004

In-situ Atomic Layer Deposition growth of Hafnium oxide

K. Karavaev, M. Tallarida, D. Schmeisser in H.T. Vierhaus (Eds.): Computer
Science Reports 03/07: DEDIS NANO DAYS. S. 13-19.
BTU Cottbus (2007), ISSN: 1437-7969

List of Symbols and Abbreviations

Abbreviation	Description
ALD	atomic layer deposition
ALE	atomic layer epitaxy
CMOS	complimentary metal oxide semiconductor
CVD	chemical vapor deposition
DRAM	dynamic random access memory
E_b	bindin energy
E_k	kinetic energy
E_g	band gap energy
EOT	equivalent oxide thickness
FET	field effect transistor
FinFET	fin field effect transistor
GDS	gas delivery system
GPC	growth per cycle
IL	interfacial layer
ITFET	inverted T channel field effect transistor
ML	monolayer
MOCVD	metalorganic chemical vapour deposition
PVD	physical vapour deposition
RT	room temperature
SR	synchrotron radiation
TDMAHf	tetra[dimethylamido]hafnium
TEMAHf	tetra[ethylmethylamino]hafnium
TFEL	thin-film electroluminescent
UHV	ultra high vacuum
VB	valence band
VBM	valence band maximum
XAS	X-ray absorption spectroscopy
XPS	X-ray photoelectron spectroscopy

Abbreviation	Description
XRF	X-ray fluorescence
XRR	X-ray reflectivity

List of Figures

1.1	Schematic cross-section of the traditional MOSFET transistor	2
2.1	Schematic illustration of an ALD cycle of a Hf-oxide process where HfCl ₄ precursors and H ₂ O are alternately pulsed and separated by inert N ₂ gas pulsing	10
2.2	Different types of growth rate vs. precursor pulse time curves in ALD processes at a constant temperature	11
2.3	Factors limiting the self-limiting growth at various temperatures	11
2.4	Schematic illustration of an XPS experiment with excitation of electrons and following their analyzing and detection	12
2.5	Sample structure. Infinitely thick homogeneous sample	13
2.6	Sample structure. The sample consisting of a thin homogeneous layer on substrate	13
2.7	Sample structure. The sample consisting of a thin island layer on substrate	13
2.8	Absorption geometry of HfO ₂ molecules on SiO ₂ /Si substrate	14
3.1	(A) The Gas Line System for ALD process with 3 lines: purging (line 1), precursor (line 2) and oxygen source (line 3) (B) The Gas Line System for ALD process for two precursors. The lines 1 and 2 are precursor source with independent purging gas. The line 3 is oxygen source. The black arrows show the direction of a gas flow.	16
3.2	Pressure behavior in the ALD reactor during usual ALD cycle (A). Time of precursor, oxygen and purging pulses (B and C)	16
3.3	Diagram of in-situ XPS and XAS system with attached ALS reactor at BESSY	18
3.4	Molecular of HfCl ₄	20
3.5	Molecular of TEMA Hf	20
3.6	Molecular of TDMA Hf	20

4.1	Ex-situ VB spectra for industrial Hf-oxide layer. The spectra were measured with photon energy of 200 eV. The major features of the VB and the core level lines are indicated.	22
4.2	Ex-situ O1s spectra for industrial Hf-oxide layer. The spectra were measured with photon energy of 800 eV.	22
4.3	Ex-situ Si2p spectra for industrial Hf-oxide layer. The spectra were measured with photon energy of 800 eV.	23
4.4	Structure of the ex-situ investigated sample.	23
4.5	Si2p spectra for HfCl ₄ (a) and TDMAHf (b). Black lines are the clean substrate, color lines are after complete ALD cycle. The spectra were measured with photon energy of 150 eV. The peaks at about 99.5 eV are due to bulk Si component, and the peaks at about 103.5 eV are due to the SiO ₂ component from the substrate. The features between 100 and 103 eV are due to the suboxide components.	24
4.6	VB spectra for HfCl ₄ (a) and TDMAHf (b). Black lines are the clean substrate, color lines are after complete ALD cycle. The spectra were measured with photon energy of 150 eV. The major features of the VB and the core level lines are indicated.	24
4.7	O1s spectra for HfCl ₄ (a) and TDMAHf (b). Black lines are the clean substrate, color lines are after complete ALD cycle. The spectra were measured with photon energy of 600 eV and 640 eV for HfCl ₄ and TDMAHf respectively.	25
4.8	Hf4d spectra for HfCl ₄ (a) and TDMAHf (B). The background, due to the Si2s plasmon tail from the substrate, was subtracted. The spectra were measured with photon energy of 600 eV and 640 eV for HfCl ₄ and TDMAHf respectively.	25
4.9	The fit Si2p spectra of etched Si/SiO ₂ substrate using a Levenberg-Marquardt least-square algorithm using Voigt functions.	27
4.10	The fit O1s spectra after 6 ALD cycle with HfCl ₄ precursor	27
4.11	Si2p intensity of the bulk Si and Si ⁺⁴ components as function of the ALD cycle using HfCl ₄ precursor. The intensity values are reported on a logarithmic scale.	28
4.12	Si2p intensity of the bulk Si and Si ⁺⁴ components as function of the ALD cycle using TDMAHf precursor. The intensity values are reported on a logarithmic scale.	28
4.13	The close line is Si2p intensity of the bulk Si component as function of the ALD cycle using HfCl ₄ precursor. The dash line is the theoretical exponential attenuation. The intensity values are reported on a logarithmic scale.	31

4.14	The close line is Si2p intensity of the bulk Si component as function of the ALD cycle using TDMAHf precursor. The dash line is the theoretical exponential attenuation. The intensity values are reported on a logarithmic scale.	31
4.15	O/Hf, Cl/Hf and (O+Cl)/Hf atomic ratios calculated from the intensities (peak area) of the O1s, Hf4d and Cl2p core level lines in HfCl ₄ experiment	32
4.16	O/Hf atomic ratio calculated from the intensities (peak area) of the O1s and Hf4d in TDMAHf experiment	32
4.17	Growth model used for calculating the O/Hf ratio in the first and second layer.	33
4.18	TEY spectra at the O1s edge of clean substrate (black line) and after each ALD cycle with HfCl ₄ precursor up to the eight (dark blue line) The raw spectra were divided by the incoming photon flux and then linear background was subtracted.	34
4.19	Integral intensity (red line) and S/B ratio (black line) values of the O1s TEY for the clean substrate and after each ALD deposition cycle. The increase of the TEY integral intensity is almost linear up to the fifth cycle and then changes at the sixth cycle. Between sixth and eighth cycles, the increase is again linear but steeper.	34
4.20	Peak the of the Cl2p for each ALD cycle for the HfCl ₄ experiment.	36
4.21	Intensity of O1s core levels of Hf-oxide component for each ALD cycle for the HfCl ₄ experiment.	36
4.22	Representation of the two ligand-exchange geometries.	37
4.23	Intensity of Hf4d core levels of Hf-oxide component for each ALD cycle for the HfCl ₄ experiment.	38
4.24	Spectra of O1s core levels for substrate (black line), after the precursor and oxidation pulses (close and dot color line, respectively) for TEMAHf experiment.	39
4.25	Spectra of VB core levels for substrate (black line), after the precursor and oxidation pulses (close and dot color line, respectively) for TEMAHf experiment.	39
4.26	Spectra of Si2p core levels for substrate (black line), after the precursor and oxidation pulses (close and dot color line, respectively) for TEMAHf experiment.	40
4.27	Spectra of C1s core levels for substrate (black line), after the precursor and oxidation pulses (close and dot color line, respectively) for TEMAHf experiment.	40

List of Tables

3.1	The parameters of the experiments with different precursors	20
4.1	Calculated ratio between Si^{+4} and Si^{+0} components of Si2p spectra, total thickness of interfacial layer t_{IL} and IL growth G_{IL} during ALD for the etched substrate and after the each ALD cycle for the HfCl_4 and after each two cycles for the TDMAHf.	29
4.2	Calculated ratio between intensity of Hf4d core level and HfO_2 component of the O1s core after the each ALD cycle for the HfCl_4 and after the each two cycles for the TDMAHf.	32